bioRxiv preprint doi: https://doi.org/10.1101/2023.11.06.565833; this version posted January 5, 2025. The copyright holder for this preprint (which was not certified by peer review) is the author/funder, who has granted bioRxiv a license to display the preprint in perpetuity. It is made available under aCC-BY 4.0 International license.

Title: Progressively shifting patterns of co-modulation among premotor cortex neurons carry dynamically similar signals during action execution and observation

Authors: Zhonghao Zhao[1] and Marc H. Schieber[1,2,3*]

Affiliations:
[1]Department of Biomedical Engineering, University of Rochester, Rochester, NY, 14627
[2]Department of Neurology, University of Rochester, Rochester, NY, 14642
[3]Department of Neuroscience, University of Rochester, Rochester, NY 14642

***Corresponding Author:**
Marc H. Schieber
E-mail: mschiebe@ur.rochester.edu

Number of:

Pages -	40
Figures -	8 (+7 figure supplements)
Tables -	2
Multimedia -	0
3D models -	0

Words in:

Abstract -	273
Introduction -	1423
Discussion -	2392

Conflict of interest:

The authors declare no conflicts of interest.

Acknowledgements:

The authors thank John Housel and Jennifer Gardinier for technical assistance, Gil Rivlis for custom task-control software, and Marsha Hayles for editorial comments. This work was supported by grant R01NS102343 (MHS) from the National Institute of Neurological Disorders and Stroke.

bioRxiv preprint doi: https://doi.org/10.1101/2023.11.06.565833; this version posted January 5, 2025. The copyright holder for this preprint (which was not certified by peer review) is the author/funder, who has granted bioRxiv a license to display the preprint in perpetuity. It is made available under aCC-BY 4.0 International license.

ABSTRACT

Many neurons in the premotor cortex show firing rate modulation whether the subject performs an action or observes another individual performing a similar action. Although such "mirror neurons" have been thought to have highly congruent discharge during execution and observation, many if not most actually show non-congruent activity. Studies of neuronal populations active during both execution and observation have shown that the most prevalent patterns of co-modulation—captured as neural trajectories—pass through subspaces which are shared in part, but in part are visited exclusively during either execution or observation. These studies focused on reaching movements for which low-dimensional neural trajectories exhibit comparatively simple dynamical motifs. But the neural dynamics of hand movements are more complex. We developed a novel approach to examine prevalent patterns of co-modulation during execution and observation of a task that involved reaching, grasping, and manipulation. Rather than following neural trajectories in subspaces that contain their entire time course, we identified time series of instantaneous subspaces, calculated principal angles among them, sampled trajectory segments at the times of selected behavioral events, and projected those segments into the time series of instantaneous subspaces. We found that instantaneous neural subspaces most often remained distinct during execution versus observation. Nevertheless, latent dynamics during execution and observation could be partially aligned with canonical correlation, indicating some similarity of the relationships among neural representations of different movements relative to one another during execution and observation. We also found that during action execution, mirror neurons showed consistent patterns of co-modulation both within and between sessions, but other non-mirror neurons that were modulated only during action execution and not during observation showed considerable variability of co-modulation.

bioRxiv preprint doi: https://doi.org/10.1101/2023.11.06.565833; this version posted January 5, 2025. The copyright holder for this preprint (which was not certified by peer review) is the author/funder, who has granted bioRxiv a license to display the preprint in perpetuity. It is made available under aCC-BY 4.0 International license.

INTRODUCTION

Although the premotor (PM) and primary motor cortex (M1) are generally thought to be involved in the planning and execution of movement, many neurons in these areas have been found to discharge not only when the subject executes a movement, but also when the subject observes a similar movement being performed by another individual. Such neurons have been found in the ventral premotor cortex (PMv) (Bonini et al., 2014; Gallese et al., 1996), dorsal premotor cortex (PMd) (Cisek and Kalaska, 2004; Papadourakis and Raos, 2019; Albertini et al., 2021; Pezzulo et al., 2022), and M1 (Dushanova & Donoghue, 2010; Kraskov et al., 2014a; Vigneswaran et al., 2013). The prevalence of such execution/observation neurons in cortical motor areas argues against their activity during observation being merely an epiphenomenon unrelated to their activity during execution, but also poses a larger question: what is the nature of the relationship between their activity during execution versus observation?

Early studies of these neurons emphasized those with congruent discharge during execution and observation contexts. Congruent neurons discharged during the same type of grasp (Gallese et al., 1996; Rizzolatti et al., 1996) or retained the same preferred direction (Dushanova & Donoghue, 2010; Kilner & Lemon, 2013) during both execution and observation. Emphasis on such congruent neurons led to the notion that they mediate understanding of observed actions as they mirror their own activity during execution (di Pellegrino et al., 1992; Rizzolatti and Craighero, 2004).

In addition to congruent neurons, however, even early studies also reported many other noncongruent neurons that also discharged during execution and during observation, but discharged differently in the two contexts (Gallese et al., 1996). In many studies roughly half or more of the neurons modulated during both execution and observation were noncongruent (Dushanova and Donoghue, 2010; Kraskov et al., 2014; Mazurek et al., 2018; Jiang et al., 2020). Of PMv neurons modulated during both execution and observation, over the time course of behavioral trials only ~20% showed brief periods with strictly congruent firing rates (Pomper et al., 2023). And in both PMv and PMd, the proportion of congruent neurons may not be different from that expected by chance alone (Papadourakis and Raos, 2019). Though many authors apply the term mirror neurons strictly to highly congruent neurons, here we will refer to all neurons modulated during both contexts—execution and observation—as mirror neurons (MNs).

That so many mirror neurons are active differently during action execution versus observation calls into question not only the extent to which the representation of movements by these neuron populations actually matches in the two contexts, but also the extent to which mirror neuron activity during observation has any meaningful function for the organism (Hickok, 2009; Krakauer et al., 2017). Nevertheless, multiple studies have found that of the neurons in cortical motor areas that are modulated during execution, a large fraction are also modulated during observation. For example, 31 of 64 (49%) pyramidal tract neurons (PTNs) in PMv and 65 of 132 (49%) in M1 showed modulation during both execution and observation (Kraskov et al., 2009; Vigneswaran et al., 2013; Kraskov et al., 2014). Such findings suggest that the observation-related activity of execution-related neurons in PMv, PMd, and M1, some of which project to the spinal cord, is somehow related to the motoric functions of these cortical areas.

The widely varying degrees of congruence versus non-congruence among individual mirror neurons may obscure population-level relationships between their patterns of co-

bioRxiv preprint doi: https://doi.org/10.1101/2023.11.06.565833; this version posted January 5, 2025. The copyright holder for this preprint (which was not certified by peer review) is the author/funder, who has granted bioRxiv a license to display the preprint in perpetuity. It is made available under aCC-BY 4.0 International license.

modulation during execution and observation. Behavior evolving in time may be represented more accurately by the temporal progression of co-modulation in populations of neurons than by the temporal pattern of firing rate in single neurons (Shenoy et al., 2013; Cunningham and Yu, 2014; Vyas et al., 2020). Patterns of co-modulation can be considered in a high-dimensional neural-state space where the firing rate of each neuron is a separate, orthogonal dimension. The instantaneous, simultaneous firing rates of all *N* neurons then is a point in this space, and the time series of instantaneous points traces out a neural trajectory in time. Neural population trajectories do not visit all regions of the *N*-dimensional state-space equivalently, however. Dimensionality reduction techniques can be used to identify a small set of latent dimensions—a subspace—that captures the most prevalent patterns of co-modulation among the population of *N* neurons.

Studies of neural trajectories underlying action execution that focused on reaching movements made with the arm have revealed that rotational motifs in a low-dimensional subspace capture much of the neural population's firing rate variance (Churchland et al., 2012; Russo et al., 2020). But the M1 neural trajectories underlying grasping movements (Suresh et al., 2020) or force production at the wrist (Dekleva et al., 2024) are more complex. The latent subspaces that capture the predominant patterns of co-modulation among M1 neurons, for example, shift progressively over the time course of behavioral trials involving reaching to, grasping, and manipulating various objects at various locations (Rouse and Schieber, 2018).

A relevant but often overlooked aspect of such dynamics in neuron populations active during both execution and observation has to do with the distinction between condition-independent and condition-dependent variation in neuronal activity (Kaufman et al., 2016; Rouse and Schieber, 2018). The variance in neural activity averaged across all the conditions in a given task context is condition-independent. For example, in an 8-direction center-out reaching task, averaging a unit's firing rate as a function of time across all 8 directions may show an initially low firing rate that increases prior to movement onset, peaks during the movement, and then declines during the final hold, irrespective of the movement direction. Subtracting this condition-independent activity from the unit's firing rate during each trial gives the remaining variance, and averaging separately across trials in each of the 8 directions then averages out noise variance, leaving the condition-dependent variance that represents the unit's modulation among the 8 directions (conditions). Alternatively, condition-independent, condition-dependent, and noise variance can be partitioned through demixed principal component analysis (Kobak et al., 2016; Gallego et al., 2018). The extent to which neural dynamics occur in a subspace shared by execution and observation versus subspaces unique to execution or observation may differ for the condition-independent versus condition-dependent partitions of neural activity. Here, we tested the hypothesis that the condition-dependent activity of PM mirror neuron populations progresses through distinct subspaces during execution versus observation, which would indicate distinct patterns of co-modulation amongst mirror neurons during execution versus observation.

Because of the complexity of condition-dependent neural trajectories for movements involving the hand, we developed a novel approach. Rather than examining trajectories over the entire time course of behavioral trials, we identified time series of instantaneous PM mirror neuron subspaces covering the time course of behavioral trials. We identified separate time series for execution trials and for observation trials, both involving four different reach-grasp-manipulation (RGM) movements. Given that each subspace in these time series is

bioRxiv preprint doi: https://doi.org/10.1101/2023.11.06.565833; this version posted January 5, 2025. The copyright holder for this preprint (which was not certified by peer review) is the author/funder, who has granted bioRxiv a license to display the preprint in perpetuity. It is made available under aCC-BY 4.0 International license.

instantaneous (a snapshot in time), it captures condition-dependent variance in the neural activity among the four RGM movements while minimizing condition-independent (time-dependent) variance.

We then tested the hypothesis that the condition-dependent subspace shifts progressively over the time course of behavioral trials (Figure 1A) by calculating the principal angles between four selected instantaneous subspaces that occurred at times easily defined in each behavioral trial—instruction onset (I), go cue (G), movement onset (M), and the beginning of the final hold (H)—and every other instantaneous subspace in the time series. Initial analyses showed that condition-dependent neural trajectories for the four RGM movements tended to separate increasingly over the course of behavioral trials. We therefore additionally examined the combined effects of i) the progressively shifting subspaces and ii) the increasing trajectory separation, by decoding neural trajectory segments sampled for 100 msec after times I, G, M, and H and projected into the time series of instantaneous subspaces (Figure 1B).

Finally, we used canonical correlation to ask whether the prevalent patterns of mirror neuron co-modulation showed similar relationships among the four RGM movements during

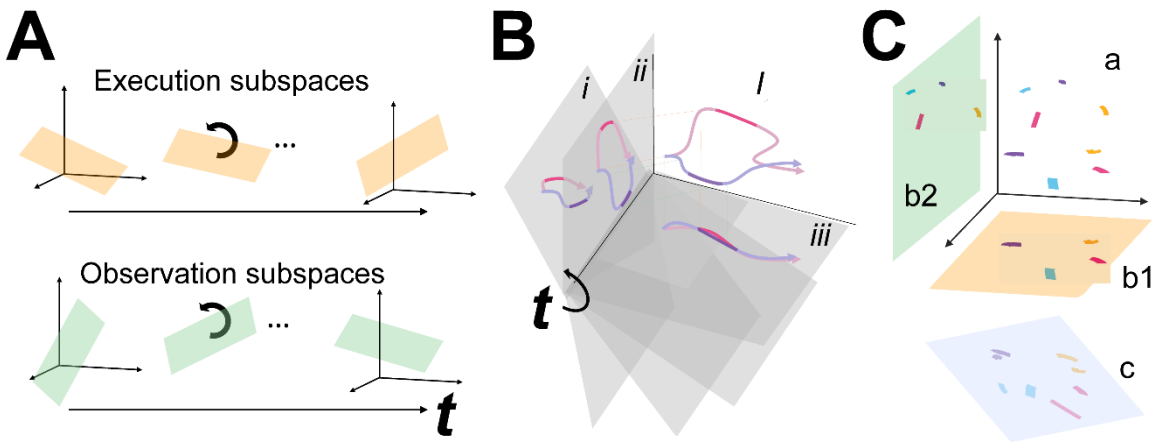

Figure 1. Conceptual approach. **A.** We hypothesized that the condition-dependent instantaneous subspace of PM MN activity shifts progressively throughout the time course of behavioral trials both during execution (orange) and during observation (green). Such shifting can be examined by calculating the principal angles between a selected instantaneous subspace and every other subspace in the time series, *t*. **B.** Segments clipped from the neural trajectories of two different movements (magenta, purple) in a high dimensional space, *I*, show varying distance between them when projected into a time series (*t* = *i, ii, iii*) of shifting, low-dimensional instantaneous subspaces (gray). This varying distance indicative of the progressive shifting of the instantaneous subspace can be followed by decoding the different movements from the trajectory segments projected into the time series of instantaneous subspaces. **C.** Neural trajectory segments from the four RGM movements (magenta, purple, cyan, and yellow) during execution and during observation originate in the same high-dimensional space (a)**,** but project into distinct low-dimensional execution (orange, b1) and observation (green, b2) subspaces. Nevertheless, canonical correlation analysis (CCA) may identify another subspace (pale blue, c) where the projected magenta, purple, cyan, and yellow segments from both execution and observation show a similar spatial relationship to one another, with the two segments of each color projecting close to one another. Such correlation between the two sets of trajectory segments projected into the same subspace would indicate similar latent dynamic relationships among the four movements during execution and observation.

bioRxiv preprint doi: https://doi.org/10.1101/2023.11.06.565833; this version posted January 5, 2025. The copyright holder for this preprint (which was not certified by peer review) is the author/funder, who has granted bioRxiv a license to display the preprint in perpetuity. It is made available under aCC-BY 4.0 International license.

166 execution and observation (Figure 1C). Such alignment would indicate that the relationships
167 among the trajectory segments in the execution subspace are similar to the relationships among
168 the trajectory segments in the observation subspace, indicating a corresponding structure in the
169 latent dynamic representations of execution and observation movements by the same PM MN
170 population. And finally, because we previously have found that during action execution the
171 activity of PM mirror neurons tends to lead that of non-mirror neurons which are active only
172 during action execution (AE neurons) (Mazurek and Schieber, 2019), we performed parallel
173 analyses of the instantaneous state space of PM AE neurons.

174

bioRxiv preprint doi: https://doi.org/10.1101/2023.11.06.565833; this version posted January 5, 2025. The copyright holder for this preprint (which was not certified by peer review) is the author/funder, who has granted bioRxiv a license to display the preprint in perpetuity. It is made available under aCC-BY 4.0 International license.

RESULTS

We recorded spiking activity as each of three monkeys executed a delayed response reach-grasp-manipulate (RGM) task, and then as each monkey observed the same task being performed by an experimenter (Figure 2A). Because we chose to study relatively naturalistic movements, the reach, grasp, and manipulation components were not performed separately, but rather in a continuous fluid motion during the movement epoch of the task sequence (Figure 2B). In previous studies involving a version of this task without separate instruction and delay epochs, we have shown that joint kinematics, EMG activity, and neuron activity in the primary motor cortex, all vary throughout the movement epoch in relation to both reach location and object grasped, with location predominating early in the movement epoch and object predominating later (Rouse and Schieber, 2015, 2016a, b). The present task, however, did not dissociate the reach, the hand shape used to grasp the object, and the manipulation performed on the object. Additional details of the behavioral task are described in the Methods. Three sessions were recorded from each of the three monkeys, R, F, and T (a 6 kg female, 10 kg male, and 10 kg male, respectively). The numbers of successful execution trials (Exe) and observation trials (Obs) involving each of the four objects—sphere, button, coaxial cylinder, and perpendicular cylinder—are given in Table 1.

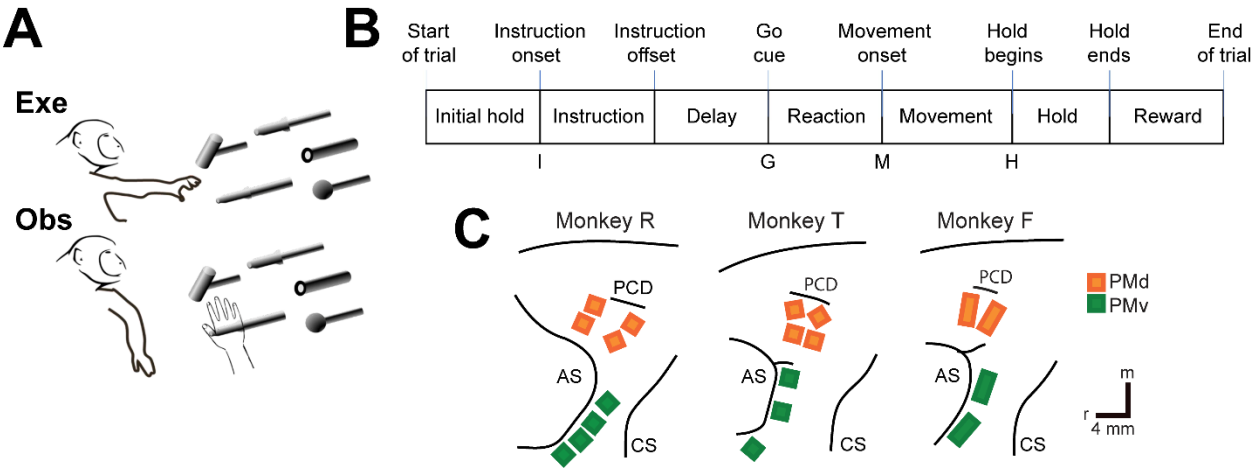

Figure 2. The reach-grasp-manipulate (RGM) task. **A.** In separate blocks of trials monkeys reached to, grasped, and manipulated four different objects themselves (Exe), and then observed a human performing the same task (Obs). **B.** The times of eight behavioral events from Start-of-trial to End-of-trial divided each trial into seven epochs from Initial hold to Reward. For analyses the data were aligned separately on, and trajectories were sampled for 100 msec following, the times of four selected events—Instruction onset (I), Go cue (G), Movement onset (M), and the beginning of the final Hold (H). **C.** Recording array locations in PMv (green) and PMd (orange) for each monkey have been redrawn from intraoperative photographs. PCD – precentral dimple; AS – arcuate sulcus; CS – central sulcus; r – rostral; m – medial. Scale bars, representing 4 mm, apply to all three monkeys.

bioRxiv preprint doi: https://doi.org/10.1101/2023.11.06.565833; this version posted January 5, 2025. The copyright holder for this preprint (which was not certified by peer review) is the author/funder, who has granted bioRxiv a license to display the preprint in perpetuity. It is made available under aCC-BY 4.0 International license.

193 **Table 1. Numbers of trials in each session**

	Monkey R		Monkey F		Monkey T	
	Exe	Obs	Exe	Obs	Exe	Obs
Session 1	(22,8,25,26)	(32,31,30,31)	(58,59,62,63)	(71,72,71,72)	(57,54,57,55)	(60,61,59,57)
Session 2	(34,26,34,38)	(40,41,40,37)	(59,58,60,56)	(73,72,75,74)	(47,53,52,43)	(57,53,58,58)
Session 3	(42,41,49,45)	(49,50,51,49)	(63,58,58,58)	(72,75,74,74)	(43,41,38,42)	(50,48,48,50)

Table 1. Numbers of trials in each session. For each of the three sessions from each of the three monkeys, numbers of trials involving each of the four objects (sphere, button, coaxial cylinder, perpendicular cylinder) are given in parentheses separately for execution and for observation.

194 The three monkeys each were implanted with Floating Microelectrode Arrays (FMAs,
195 Microprobes for Life Sciences) in the ventral premotor cortex (PMv) and in the dorsal premotor
196 cortex (PMd). The locations of the arrays in each monkey are illustrated in Figure 2C. Using
197 object and epoch as factors, we performed two-way repeated measures analysis of variance
198 (ANOVA) on the firing rate of each sorted unit recorded from the arrays in each session (see
199 Methods). Because unit firing rates typically differed during execution and observation, we
200 performed such ANOVAs separately on execution trials and observation trials. Table 2 gives the
201 numbers of PM (PMv+PMd) units identified in each session as being modulated significantly
202 during both execution and observation, which we refer to as mirror neurons (MN), along with the
203 numbers of units modulated significantly during execution but not observation (AE), during
204 observation but not execution (AO), or with no significant modulation during either execution or
205 observation (NS). The numbers of AO and NS units were consistently small across monkeys
206 and sessions. The present analyses therefore focus on MNs and, for comparison, AE neurons.

207 **Table 2. Numbers of units in each session**

Monkey	Session	MN	AE	AO	NS
R	1	48(19,29)	35(20,15)	3(1,2)	5(2,3)
	2	47(21,26)	25(16,9)	5(1,4)	11(4,7)
	3	37(19,18)	49(20,29)	1(1,0)	8(7,1)
T	1	79(37,42)	15(5,10)	2(0,2)	7(1,6)
	2	91(48,43)	22(6,16)	3(1,2)	7(1,6)
	3	100(48,52)	18(7,11)	0(0,0)	6(2,4)
F	1	44(24,20)	7(5,2)	1(1,0)	8(8,0)
	2	47(32,15)	10(9,1)	5(1,4)	3(3,0)
	3	42(28,14)	9(7,2)	3(1,2)	3(3,0)

Table 2. Numbers of PM units in each session. For each of the three sessions from each of the three monkeys (R, T, and F), numbers of PM units are given for each of four classes in the format of Total (PMv, PMd). MN – mirror neurons, modulated significantly during action execution and during action observation. AE – action execution neurons, modulated during execution but not during observation. AO – action observation neurons, modulated during observation but not execution. NS – not significant, units not modulated significantly during either execution or observation.

bioRxiv preprint doi: https://doi.org/10.1101/2023.11.06.565833; this version posted January 5, 2025. The copyright holder for this preprint (which was not certified by peer review) is the author/funder, who has granted bioRxiv a license to display the preprint in perpetuity. It is made available under aCC-BY 4.0 International license.

Condition-dependent versus condition-independent neural activity in PM MNs

Whereas a large fraction of condition-dependent neural variance during reaching movements without grasping can be captured in a two-dimensional subspace (Churchland et al., 2012; Ames et al., 2014), condition-dependent activity in movements that involve grasping is more complex (Suresh et al., 2020). In part, this may reflect the greater complexity of controlling the 24 degrees of freedom in the hand and wrist as compared to the 4 degrees of freedom in the elbow and shoulder (Sobinov and Bensmaia, 2021). Figure 3 illustrates this complexity in a PM MN population during the present RGM movements.

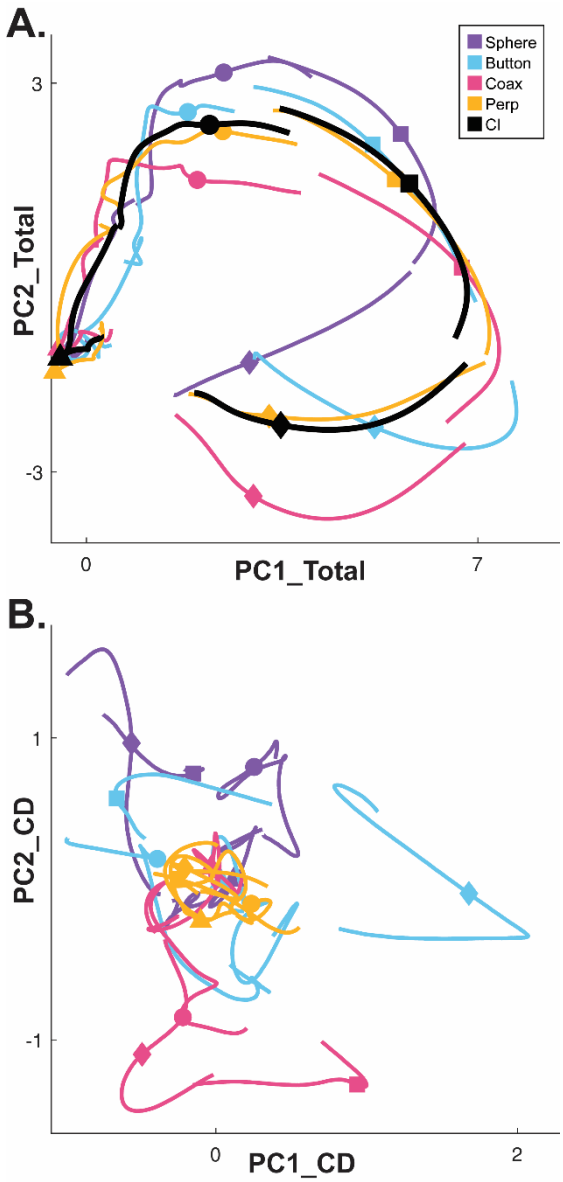

Figure 3. Neural trajectories of condition-independent versus condition-dependent activity. **A**. Neural trajectories of PM MN firing rates averaged across multiple execution trials involving each of the four objects (Sphere – purple, Button – cyan, Coaxial cylinder [Coax]– magenta, Perpendicular cylinder [Perp]– yellow) have been projected into the PC1 vs PC2 plane of the Total neural activity. Averaging these four trajectories gives their common, condition-independent (CI) trajectory (black). Time proceeds clockwise from left, with data separately aligned at four selected times: triangle – instruction onset (I); circle – go cue (G); square – movement onset (M); diamond – beginning of final hold (H). **B**. Condition-dependent trajectories obtained by subtracting the CI trajectory (black) from each of the four single-object trajectories (colors) in **A**, and then projected into the PC1 vs PC2 plane of their common, condition dependent (CD) subspace across the entire time course of trials. Data from monkey R, session 2.

Here, PCA was performed on the activity of a PM MN population across the entire time course of execution trials involving all four objects. The colored traces in Figure 3A show neural trajectories averaged separately across trials involving each of the four objects and then projected into the PC1 vs PC2 plane of the total neural space. Most of the variance in these four trajectories is comprised of a shared rotational component. The black trajectory, obtained by averaging trajectories from trials involving all four objects together, represents this condition-independent (i.e. independent of the object involved) activity. The condition-dependent (i.e. dependent on which object was involved) variation in activity is reflected by the variation in the colored trajectories around the black trajectory. The condition-dependent portions can be isolated by subtracting the black trajectory from each of the colored trajectories. The resulting four condition-dependent trajectories have been projected into the PC1 vs PC2 plane of their own common subspace in Figure 3B. Rather than exhibiting a simple rotational motif, these trajectories appear knotted. To better understand how these complex, condition-dependent

bioRxiv preprint doi: https://doi.org/10.1101/2023.11.06.565833; this version posted January 5, 2025. The copyright holder for this preprint (which was not certified by peer review) is the author/funder, who has granted bioRxiv a license to display the preprint in perpetuity. It is made available under aCC-BY 4.0 International license.

trajectories progress over the time course of RGM trials, we chose to examine time series of instantaneous subspaces.

Instantaneous subspaces shift progressively during both execution and observation

We identified an instantaneous subspace at each one millisecond time step of RGM trials. At each time step, we applied PCA to the 4 instantaneous neural states (i.e. the 4 points on the neural trajectories representing trials involving the 4 different objects each averaged across 20 trials per object, totaling 80 trials), yielding a 3-dimensional subspace at that time (see Methods). Note that because these 3-dimensional subspaces are essentially instantaneous, they capture the condition-dependent variation in neural states, but not the common, condition-independent variation. To examine the temporal progression of these instantaneous subspaces, we then calculated the principal angles between each 80-trial instantaneous subspace and the instantaneous subspaces averaged across *all* trials at four behavioral time points that could be readily defined across trials, sessions, and monkeys: the onset of the instruction (I), the go cue (G), the movement onset (M), and the beginning of the final hold (H). This process was repeated 10 times with replacement to assess the variability of the principal angles. The closer the principal angles are to 0°, the closer the two subspaces are to being identical; the closer to 90°, the closer the two subspaces are to being orthogonal.

Figure 4A-D illustrate the temporal progression of the first principal angle of the mirror neuron population in the three sessions (red, green, and blue) from monkey R during execution trials. As illustrated in Figure 4 – figure supplement 1 (see also the related Methods), in each session all three principal angles, each of which could range from 0° to 90°, tended to follow a similar time course. In the Results we therefore illustrate only the first (i.e. smallest) principal angle. Solid traces represent the mean across 10-fold cross validation using the 80-trial subsets of all the available trials; shading indicates ±1 standard deviation. As would be expected, the instantaneous subspace using 80 trials approaches the subspace using all trials at each of the four selected times—I, G, M, and H—indicated by the relatively narrow trough dipping toward 0°. Of greater interest are the slower changes in the first principal angle in between these four time points. Figure 4A shows that after instruction onset (I) the instantaneous subspace shifted quickly away from the subspace at time I, indicated by a rapid increase in principal angle to levels not much lower than what might be expected by chance alone (horizontal dashed line). In contrast, throughout the remainder of the instruction and delay epochs (from I to G), Figure 4B and C show that the 80-trial instantaneous subspace shifted gradually and concurrently, not sequentially, toward the all-trial subspaces that would be reached at the end of the delay period (G) and then at the onset of movement (M), indicated by the progressive decreases in principal angle. As shown by Figure 4D, shifting toward the H subspace did not begin until the movement onset (M). To summarize, these changes in principal angles indicate that after shifting briefly toward the subspace present at time the instruction appeared (I), the instantaneous subspace shifted progressively throughout the instruction and delay epochs toward the subspace that would be reached at the time of the go cue (G), then further toward that at the time of movement onset (M), and only thereafter shifted toward the instantaneous subspace that would be present at the time of the hold (H).

bioRxiv preprint doi: https://doi.org/10.1101/2023.11.06.565833; this version posted January 5, 2025. The copyright holder for this preprint (which was not certified by peer review) is the author/funder, who has granted bioRxiv a license to display the preprint in perpetuity. It is made available under aCC-BY 4.0 International license.

Figure 4E-H show the progression of the first principal angle of the mirror neuron population during observation trials. Overall, the temporal progression of the MN instantaneous subspace during observation was similar to that found during execution, particularly around times I and H. The decrease in principal angle relative to the G and M instantaneous subspaces during the delay epoch was less pronounced during observation than during

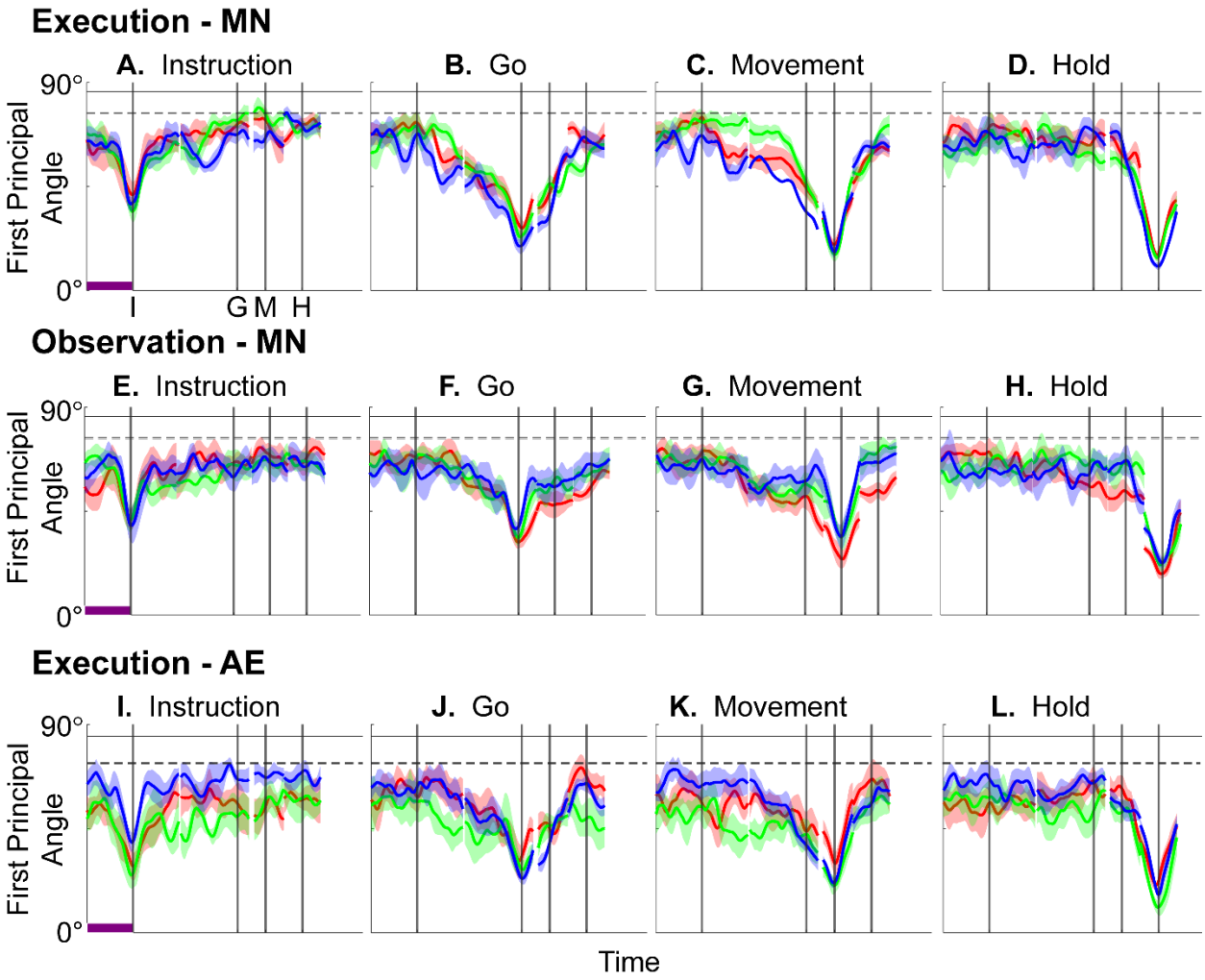

Figure 4. Time course of the first principal angle between instantaneous subspaces. **A – D:** MN populations during execution trials; **E – H:** MN populations during observation trials; **I – L:** AE neuron populations during execution trials. Each frame shows the time course of the first principal angle between the time series of instantaneous subspaces and that present at one of four selected times—**A, E, I:** instruction onset; **B, F, J:** go cue; **C, G, K:** movement onset; or **D, H, L:** the beginning of the final hold. Results in 1 ms steps have been aligned separately at the times of the instruction onset (I), go cue (G), movement onset (M), and hold (H)—each indicated by a vertical line as labeled in the frame at upper left. Red, green, and blue traces represent sessions 1, 2, and 3, respectively, from monkey R. Solid traces represent means and shaded areas represent ±1 standard deviation across 10-fold cross validation as described in the Methods. Horizontal black lines indicate the average (solid) and the average minus 3 standard deviations (dashed) of the first principal angle between a fixed 3D space and other 3D spaces chosen randomly within a *N*-dimensional space (see Figure 4 – figure supplement 2 and related Methods). Here $N = 37$, the number of MNs in session 3. Horizontal purple bars in the left column (**A, E, I**) indicate 500 ms, which applies to the entire row.

bioRxiv preprint doi: https://doi.org/10.1101/2023.11.06.565833; this version posted January 5, 2025. The copyright holder for this preprint (which was not certified by peer review) is the author/funder, who has granted bioRxiv a license to display the preprint in perpetuity. It is made available under aCC-BY 4.0 International license.

execution. Nevertheless, these findings support the hypothesis that the condition-dependent subspace of PM MNs shifts progressively over the time course of RGM trials during both execution and observation, as illustrated schematically in Figure 1A.

We also examined the temporal progression of the instantaneous subspace of AE neurons. As would be expected given that AE neurons were not modulated significantly during observation trials, in the observation context AE populations had no gradual changes in principal angle (Figure 4 – figure supplement 3). During execution, however, Figure 4I-L show that the AE populations had a pattern of gradual decrease in principal angle similar to that found in the MN population (Figure 4A-D). After the instruction onset, the instantaneous subspace shifted quickly away from that present at time I and progressed gradually toward that present at times G and M, only shifting toward that present at time H after movement onset. As for the PM MN populations, the condition-dependent subspace of the PM AE populations shifted progressively over the time course of execution RGM trials.

Neural trajectories separate progressively during both execution and observation

The progressive changes in principal angles do not capture another important aspect of condition-dependent neural activity. The neural trajectories during trials involving different objects separated increasingly as trials progressed in time. To illustrate this increasing separation, we clipped 100 ms segments of high-dimensional MN population trial-averaged trajectories beginning at times I, G, M, and H, for trials involving each of the four objects. We then projected the set of four object-specific trajectory segments clipped at each time into each of the four instantaneous 3D subspaces at times I, G, M, and H. This process was repeated separately for execution trials and for observation trials.

For visualization, we projected these trial-averaged trajectory segments from an example session into the PC1 vs PC2 planes (which consistently captured > 70% of the variance) of the I, G, M, or H instantaneous 3D subspaces. In Figure 5, the trajectory segments for each of the four objects (sphere – purple, button – cyan, coaxial cylinder – magenta, perpendicular cylinder – yellow) sampled at different times (rows) have been projected into each of the four instantaneous subspaces defined at different times (columns). Rather than appearing knotted as in Figure 3, these short trajectory segments are distinct when projected into each instantaneous subspace.

Along the main diagonal of Figure 5A, each set of trajectory segments is projected into its corresponding subspace, showing that during execution the trajectory segments for the four objects were close together at the time of instruction onset (I), beca,e more separated at the time of the go cue (G), had separated further still at movement onset (M), and had become somewhat less separated at the beginning of the final hold (H). During observation (Figure 5B) a similar trend is evident along the main diagonal, although the separation is less, reflecting the commonly described lower firing rates of MNs during observation than during execution (Ferroni et al., 2021). In addition, during observation the separation of the four trajectories was somewhat greater at the beginning of the hold (H) than at movement onset (M). Off-diagonal frames along the rows (same trajectory segments, different instantaneous subspaces) or along the columns (different trajectory segments, same instantaneous subspaces) show less separation than along the main diagonal, both during execution and during observation. To summarize these differences in trajectory separation, we calculated the 3-dimensional cumulative separation (*CS* – see Methods) for each set of four segments projected into each of

bioRxiv preprint doi: https://doi.org/10.1101/2023.11.06.565833; this version posted January 5, 2025. The copyright holder for this preprint (which was not certified by peer review) is the author/funder, who has granted bioRxiv a license to display the preprint in perpetuity. It is made available under aCC-BY 4.0 International license.

the four instantaneous subspaces both for this example session and averaged across all 9 sessions (Figure 5 – figure supplement 1). These differences in separation when the same trajectory segments are projected into different subspaces reflect the progressive shifting of the condition-dependent instantaneous subspace of the PM MN population as trials progressed in time, illustrated schematically in Figure 1B.

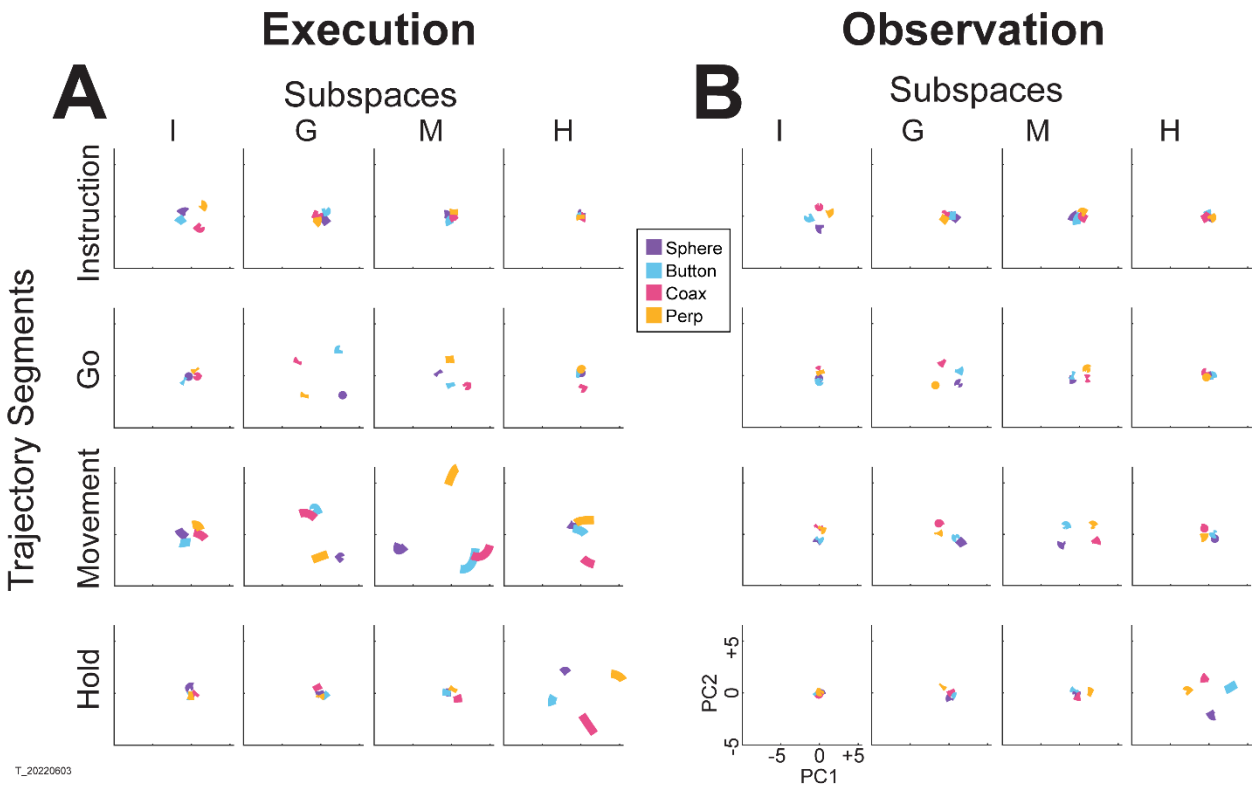

Figure 5. MN trajectory segments projected into instantaneous subspaces**. A.** Using execution data from an example session (monkey T, session 3), trajectory segments averaged across trials involving each of the four objects (sphere – purple, button – cyan, coaxial cylinder [coax] – magenta, perpendicular cylinder [perp] – yellow) were clipped for 100 ms immediately following each of four behavioral events (rows: Instruction onset, Go cue, Movement onset, Hold). Each set of these four segments then was projected into the PC1 vs PC2 plane of the instantaneous 3D subspace present at four different times (columns: I, G, M, H). **B.** The same process was performed using observation data from the same session. The PC1 vs PC2 scales at lower left in **B** apply to all frames in both **A** and **B**.

Decodable information changes progressively during both execution and observation

As RGM trials proceeded in time, the condition-dependent neural activity of the PM MN population thus changed in two ways. First, the instantaneous condition-dependent subspace shifted, indicating that the patterns of firing-rate co-modulation among neurons representing the four different RGM movements changed progressively, both during execution and during observation. Second, as firing rates generally increased, the neural trajectories representing the four RGM movements became progressively more separated, more so during execution than during observation.

bioRxiv preprint doi: https://doi.org/10.1101/2023.11.06.565833; this version posted January 5, 2025. The copyright holder for this preprint (which was not certified by peer review) is the author/funder, who has granted bioRxiv a license to display the preprint in perpetuity. It is made available under aCC-BY 4.0 International license.

To evaluate the combined effects of these two progressive changes, we clipped 100 ms single-trial trajectory segments beginning at times I, G, M, or H, and projected these trajectory segments from individual trials into the instantaneous 3D subspaces at 50 ms time steps. At each of these time steps, we trained a separate LSTM decoder to classify individual trials according to which of the four objects was involved in that trial. We expected that the trajectory segments would be classified most accurately when projected into instantaneous subspaces near the time at which the trajectory segments were clipped. At other times we reasoned that classification accuracy would depend both on the similarity of the current instantaneous subspace to that found at the clip time as evaluated by the principal angle (Figure 4), and on the separation of the four trajectories at the clip time (Figure 5).

Figure 6A-D shows the resulting classification accuracy as a function of trial time for the 100 ms Instruction, Go, Movement, or Hold mirror-neuron execution trajectory segments, each projected into the same time series of instantaneous mirror-neuron execution subspaces from the same session. Solid curves indicate classification accuracy averaged across 10-fold cross-validation (as described in the Methods); the surrounding shaded areas indicate ± 1 standard deviation from that average; different colors indicate results from the three different sessions in monkey R. Horizontal lines indicate the range of classification accuracies that would have been obtained had the instantaneous subspaces been chosen randomly, which we estimated for each set of trajectory segments by bootstrapping—projecting the trajectory segments into a randomly selected 3D space, training an LSTM decoder, and classifying single trials, repeated 500 times (Natraj et al., 2022).

As might have been expected based both on principal angles and on trajectory separation, classification accuracy consistently peaked at a time point within or near the 100 ms duration of the corresponding trajectory segments (orange flags at the top of the vertical lines). Classification accuracy decreased progressively at times preceding and following each of these peaks. In monkey R, mean classification of the Instruction trajectory segments (Figure 6A) initially was ~0.25, rose toward ~0.50 around the time of the instruction onset, and then fell back to ~0.25. Mean accuracy for the Go segments (Figure 6B) also began at ~0.25, rose gradually during the delay epoch to peak at ~0.75 around the time of the Go cue, and decreased thereafter. For the Movement (Figure 6C) and Hold (Figure 6D) segments, classification accuracy started somewhat higher (reflecting greater trajectory segment separation at the time they were clipped, Figure 5) and peaked at ~0.90. Similar trends were seen for monkeys T and F. For each monkey, classification accuracy for each of the four sets of trajectory segments—Instruction, Go, Movement, and Hold—as a function of time was relatively consistent across sessions.

Although classification accuracy consistently peaked near the behavioral event at which time each set of trajectory segments was clipped, the rise in accuracy before and the decline after the peak differed depending on the behavioral event. Peak classification accuracy for Instruction segments was modest, beginning to rise from mean chance levels ~100 ms before the instruction onset, and quickly falling back thereafter (Figure 6A). At times outside of this brief peak, however, the instantaneous subspace was no more similar to that at the time of instruction onset than would be expected from chance alone.

bioRxiv preprint doi: https://doi.org/10.1101/2023.11.06.565833; this version posted January 5, 2025. The copyright holder for this preprint (which was not certified by peer review) is the author/funder, who has granted bioRxiv a license to display the preprint in perpetuity. It is made available under aCC-BY 4.0 International license.

In contrast, classification accuracy for the Go trajectory segments (Figure 6B) was elevated above mean chance levels for more of the RGM trial duration. Though exceeding 3 standard deviations from mean chance only late in the delay epoch, Go-segment classification accuracy rose steadily through the delay epoch, peaked near the go cue, then fell back to near

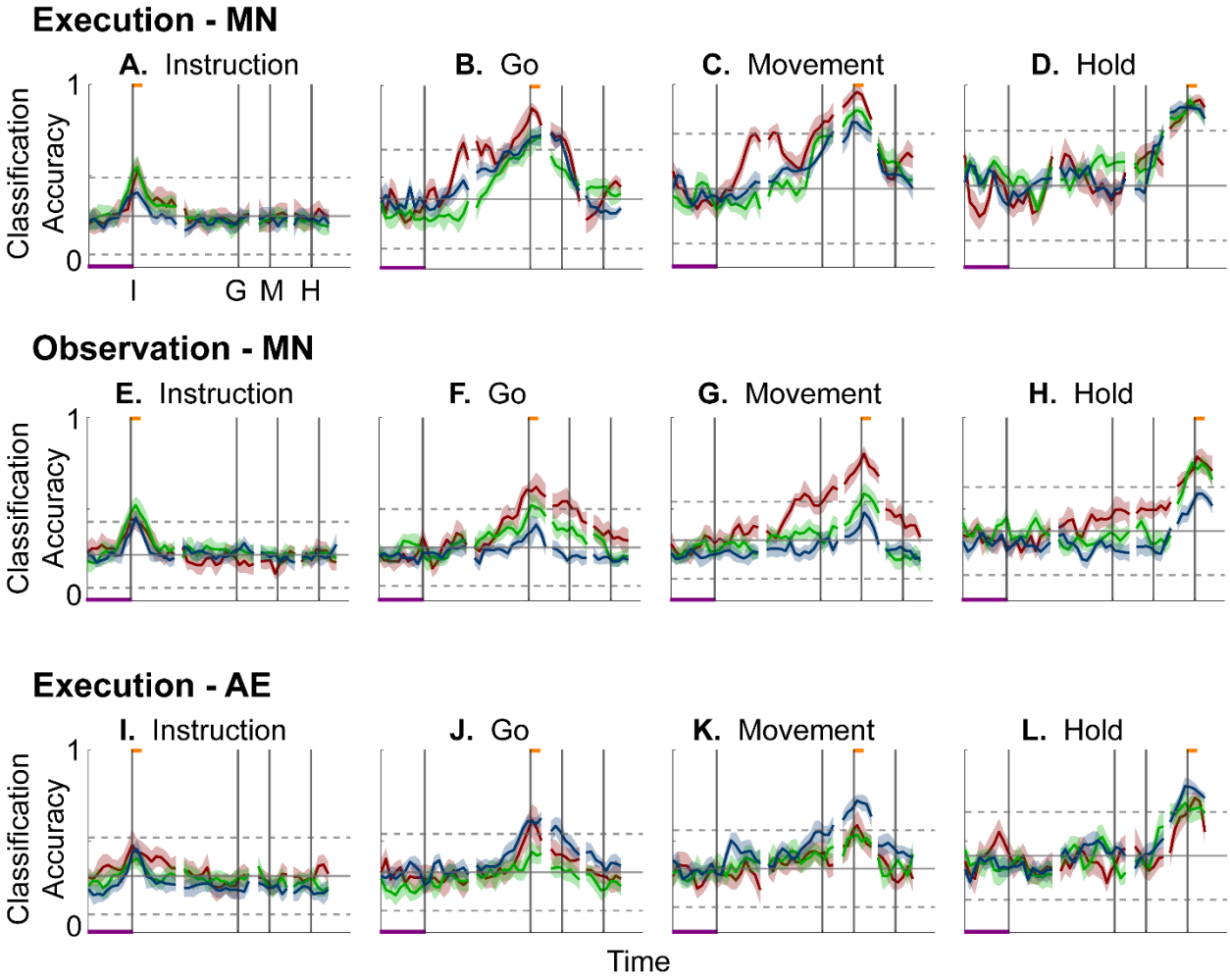

Figure 6. Decodable information as a function of time. **A – D:** Classification accuracy for mirror-neuron execution trajectory segments projected into instantaneous execution subspaces; **E – H:** for mirror-neuron observation trajectory segments projected into their instantaneous observation subspaces**; I-L:** for action-execution neuron trajectory segment projected into their instantaneous execution subspaces. **A, E, I:** Instruction trajectory segments; **B, F, J:** Go segments; **C, G, K:** Movement segments; **D, H, L:** Hold segments. Red, green, and blue traces represent sessions 1, 2, and 3, respectively, from monkey R. Results in 50 ms steps have been aligned separately at the times of the instruction onset (I), go cue (G), movement onset (M), and hold (H)—each indicated by a vertical line as labeled in the frame at upper left. In each frame, the short horizontal orange flag at the top of the vertical lines indicates the 100 ms during which each set of trajectory segments was clipped; the horizontal purple bar at lower left represents 500 ms. Solid curves indicate mean classification accuracy across 10-fold cross validation as a function of time, with the shaded areas indicating 1 standard deviation. Horizontal black lines indicate the mean (solid) ± 3 standard deviations (dashed) classification accuracy obtained by projecting each set of trajectory segments into 500 randomly selected 3D spaces.

bioRxiv preprint doi: https://doi.org/10.1101/2023.11.06.565833; this version posted January 5, 2025. The copyright holder for this preprint (which was not certified by peer review) is the author/funder, who has granted bioRxiv a license to display the preprint in perpetuity. It is made available under aCC-BY 4.0 International license.

mean chance levels during the reaction (G to M) and movement (M to H) epochs. Likewise, the rise in classification accuracy of Movement trajectory segments (Figure 6C) also began, not after the go cue, but earlier, in the middle of the delay epoch (I to G). Movement-segment classification accuracy rose steadily from the second half of the delay epoch through the reaction epoch (G to M), peaked above chance levels shortly after movement onset (M), and fell back to near baseline during the movement epoch (M to H). Had the condition-dependent instantaneous subspaces during the delay epoch been orthogonal to those at the time of movement onset, the Movement trajectory segments would have had no projection in delay epoch subspaces and classification accuracy would have remained at baseline. The progressive increase in classification accuracy of Movement trajectory segments during the preparatory delay and reaction epochs indicates that as these epochs proceeded the condition-dependent neural trajectories of PM MNs shifted gradually, not abruptly, toward where they would be at movement onset.

Classification accuracy of the Hold trajectory segments (Figure 6D) increased relatively late in execution trials. During the instruction, delay, and reaction epochs the instantaneous subspaces were no more similar than chance to that at the beginning of the hold epoch. Classification accuracy of Hold trajectory segments began to increase only after movement onset (M), rising through the movement epoch, peaking near the beginning of the hold epoch and decreasing thereafter.

We performed a similar classification accuracy analysis for observation trials. For Instruction trajectory segments (Figure 6E), the brief peak of classification accuracy occurring around the time of instruction onset (I) during observation trials was quite like that found during execution trials. For the Go and Movement segments (Figure 6F,G), although classification accuracy tended to be lower, a gradual rise again began during the delay epoch. Classification accuracy of the Hold trajectory segments, during observation as during execution, began to increase only after movement onset (Figure 6H).

During execution trials, classification accuracy for AE populations (Figure 6I-L) showed a time course quite similar to that for MN populations, though amplitudes were lower overall, most likely because of the smaller population sizes. During observation, AE populations showed only low-amplitude, short-lived peaks of classification accuracy around times I, G, M, and H (Figure 6 – figure supplement 1). Given that individual AE neurons showed no statistically significant modulation during observation trials, even these small peaks might not have been expected. Previous studies have indicated, however, that neurons not individually related to task events nevertheless may contribute to a population response (Shenoy et al., 2013; Cunningham and Yu, 2014; Gallego et al., 2017; Jiang et al., 2020).

bioRxiv preprint doi: https://doi.org/10.1101/2023.11.06.565833; this version posted January 5, 2025. The copyright holder for this preprint (which was not certified by peer review) is the author/funder, who has granted bioRxiv a license to display the preprint in perpetuity. It is made available under aCC-BY 4.0 International license.

Do PM mirror neurons progress through the same subspaces during execution and observation?

Having found that PM mirror neuron populations show similar progressive shifts in their instantaneous neural subspace during execution and observation of RGM trials, as well as similar changes in decodable information, we then asked whether this progression passes through similar subspaces during execution and observation. To address this question, we first calculated the principal angles between the instantaneous mirror-neuron *execution* subspace at selected times I, G, M, or H and the entire time series of instantaneous mirror-neuron *observation* subspaces (Figure 7A-D). Conversely, we calculated the principal angles between the instantaneous *observation* subspaces at selected times I, G, M, or H and the entire time series of instantaneous *execution* subspaces (Figure 7E-H). Although the principal angles were slightly smaller than might be expected from chance alone, indicating some minimal overlap of execution and observation instantaneous subspaces, the instantaneous observation subspaces did not show any progressive shift toward the I, G, M, or H execution subspace (Figure 7A-D), nor did the instantaneous execution subspaces shift toward the I, G, M, or H observation subspace (Figure 7E-H). We also used classification accuracy to evaluate cross-projected trajectory segments and again found little evidence of overlap between execution and observation subspaces (Figure 7 – figure supplement 1). Although monkey T did show evidence of some degree of overlap (Figure 7 – figure supplement 2), throughout the time

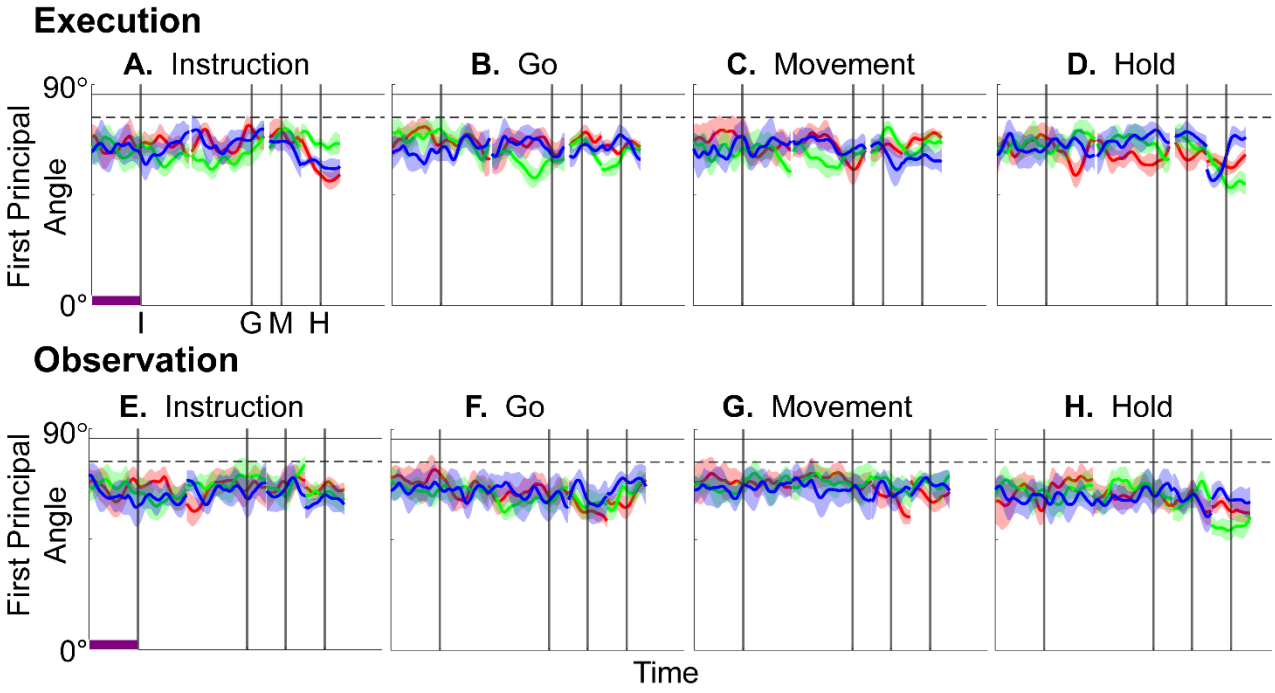

Figure 7. Time course of the first principal angle cross-calculated between instantaneous execution and observation subspaces of PM MNs as a function of time. First principal angles between the instantaneous *execution* subspace at selected times I, G, M, or H and the entire time series of instantaneous *observation* subspaces are shown above (**A-D**); between the instantaneous *observation* subspace at selected times I, G, M, or H and the entire time series of instantaneous *execution* subspaces below (**E-H**). Formatting is the same as in Figure 4.

bioRxiv preprint doi: https://doi.org/10.1101/2023.11.06.565833; this version posted January 5, 2025. The copyright holder for this preprint (which was not certified by peer review) is the author/funder, who has granted bioRxiv a license to display the preprint in perpetuity. It is made available under aCC-BY 4.0 International license.

course of trials in in monkeys R and F, the instantaneous execution and observation condition-dependent subspaces showed little if any overlap.

Alignment of latent dynamics

We next asked whether mirror neuron execution and observation trajectory segments, though progressing through distinct subspaces, nevertheless could be aligned using canonical correlation analysis (CCA) to project both sets of trajectory segments into another, common subspace, as illustrated schematically in Figure 1C. Such alignment would indicate that neural representations of trials involving the four objects bore a similar relationship to one another in neural space during execution and observation, even though they occurred in different subspaces. For example, the trajectories of PMd+M1 neuron populations recorded from two different monkeys during center-out reaching movements could be aligned well (Safaie et al., 2023). CCA showed, for example, that in both brains the neural trajectory for the movement to the target at 0° was closer to the trajectory for movement to the target at 45° than to the trajectory for the movement to the target at 180°. Relationships among these latent dynamic representations of the eight movements thus were similar even though the neural populations were recorded from two different monkeys.

We therefore applied CCA (see Methods) to align the trajectory segments of execution trials with those of observation trials. As an example, trial-averaged Hold execution trajectory segments in their original execution subspace at time H, and Hold observation trajectory segments in their original observation subspace at time H, are shown in Figure 8A. The relationships among the execution trajectory segments appear substantially different than that among the observation trajectory segments. But when both sets of trajectory segments are projected into another common subspace identified with CCA, as shown in Figure 8B, a similar relationship among the neural representations of the four movements during execution and observation is revealed. In both behavioral contexts the neural representation of movements involving the sphere (purple) is now closest to the representation of movements involving the coaxial cylinder (magenta) and farthest from that of movements involving the button (cyan). The two sets of trajectory segments are more or less “aligned.”

As a positive control, we first aligned MN execution trajectory segments from two different sessions in the same monkey (which we abbreviate as MN:1/2). The 2 sessions in monkey R provided only 1 possible comparison, but the 3 sessions in monkeys T and F each provided 3 comparisons. For each of these 7 comparisons, we found the bootstrapped average of CC1, of CC2, and of CC3. The 3D means ± standard deviations of these 7 averages for the Instruction, Go, Movement, and Hold trajectory segments have been plotted in Figure 8C (black). The progressive increase in mean correlation coefficients reflects the general increase in firing rates relative to trial-by-trial variability from the early to later trial epochs. The highest values for MN:1/2 correlations were obtained for the Movement trajectory segments ($\overline{CC1} = 0.89$, $\overline{CC2} = 0.77$, $\overline{CC3} = 0.61$). These relatively high values indicate relatively consistent relationships among the Movement neural trajectory segments representing the four different RGM movements from session to session, as would have been expected from previous studies (Gallego et al., 2018; Gallego et al., 2020; Safaie et al., 2023).

bioRxiv preprint doi: https://doi.org/10.1101/2023.11.06.565833; this version posted January 5, 2025. The copyright holder for this preprint (which was not certified by peer review) is the author/funder, who has granted bioRxiv a license to display the preprint in perpetuity. It is made available under aCC-BY 4.0 International license.

481

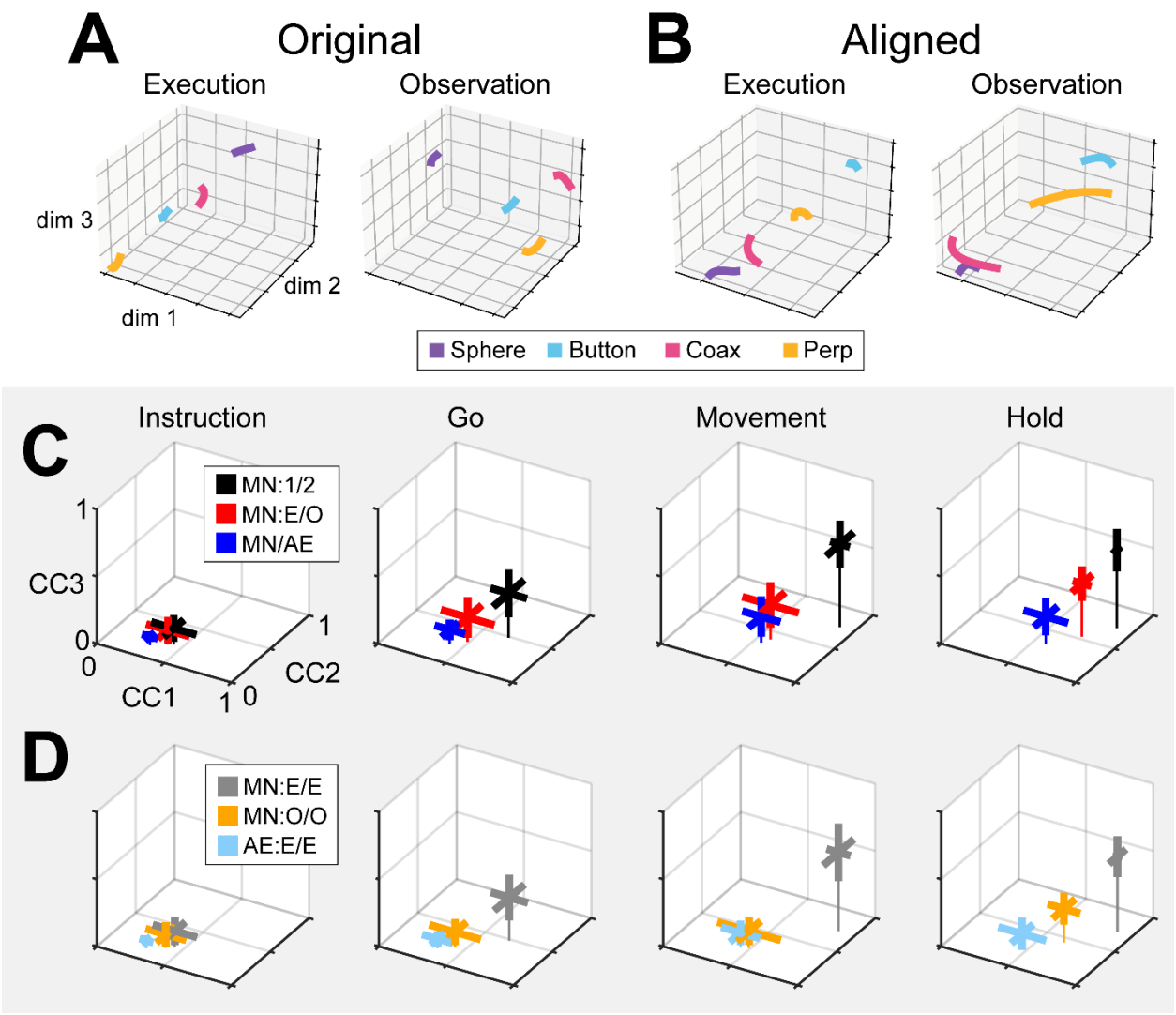

Figure 8. Alignment of trajectory segments by canonical correlation. **A.** For an example session (monkey F, session 2), mirror neuron Hold trajectory segments from execution trials have been projected into their original instantaneous execution subspace at time H (left), and from observation trials into their original instantaneous observation subspace also at time H (right). **B.** The same execution (left) and observation (right) trajectory segments all have been projected into another, common subspace identified with canonical correlation. Colors indicate trajectory segments from trials involving the sphere – purple, coaxial cylinder (coax)– magenta, perpendicular cylinder (perp) – yellow, and button – cyan. **C.** The three correlation coefficients resulting from CCA (CC1, CC2, and CC3) have been averaged across comparisons from all sessions from the three monkeys. Thick bars representing the standard deviations of the three coefficients cross at their means, with a thin line dropped vertically from that point to the CC1 vs CC2 plane. CCA of MN trajectory segments from execution trials recorded in two different sessions from the same monkey (black, MN:1/2) is used as a point of reference with which to compare alignment of MN execution versus observation trials collected in the same session (red, MN:E/O), and MN versus AE neuron execution segments from the same session (blue, MN/AE). **D.** Correlation coefficients from within-group CCA alignment for MN execution segments (gray, MN:E/E), MN observation trajectory segments (orange, MN:O/O) and AE execution segments (light blue, AE:E/E). See text for further description.

bioRxiv preprint doi: https://doi.org/10.1101/2023.11.06.565833; this version posted January 5, 2025. The copyright holder for this preprint (which was not certified by peer review) is the author/funder, who has granted bioRxiv a license to display the preprint in perpetuity. It is made available under aCC-BY 4.0 International license.

Given that PM MN activity progressed largely through non-overlapping instantaneous subspaces during execution versus observation, we proceeded to ask whether the relationship among the neural representations of the four RGM movements was similar during execution versus observation. To address this question, we aligned MN execution trajectory segments with MN observation trajectory segments from the same session (MN:E/O; 2 sessions from monkey R, 3 from monkey T, 3 from monkey F). The 3D mean ± standard deviation correlation coefficients for these 8 alignments also has been plotted in Figure 8C (red). Here, the highest values were reached for the Hold trajectory segments ($\overline{CC1} = 0.73$, $\overline{CC2} = 0.54$, $\overline{CC3} = 0.39$). Though not as high as for execution/execution alignment, these values indicate substantial alignment of MN trajectory segments from execution and observation. PM MN populations thus showed some degree of similarity in the relationships among their latent dynamic representations of the four RGM movements during execution and observation, particularly at the time of the hold.

Although MNs are known to be present in considerable numbers in both the primary motor cortex and premotor cortex (see Introduction), most studies of movement-related cortical activity in these areas make no distinction between neurons with activity only during action execution (AE neurons) and those with activity during both execution and observation (MNs). This reflects an underlying assumption that during action execution, mirror neurons function in parallel with AE neurons, differing only during observation. We therefore tested the hypothesis that MN and AE neuron execution trajectory segments from the same session would align well. Figure 8C (blue) shows the mean CCs between MN and AE execution trajectory segments across 8 alignments (MN/AE; 2 R, 3 T, 3 F), which reached the highest values for the Hold segments ($\overline{CC1} = 0.57$, $\overline{CC2} = 0.35$, $\overline{CC3} = 0.19$). All three of these coefficients were substantially lower than those for the MN execution vs. observation alignments given above. Surprisingly, the alignment of AE neuron execution trajectory segments with those of the simultaneously recorded MN population was weaker than the alignment of MN trajectories during execution vs. observation.

Statistical comparisons across the three sets of alignments illustrated in Figure 8C (MN:1/2; MN:E/O; and MN/AE) showed significant variation in each of the three CCA coefficients for each set of trajectory segments, with the exception of the Instruction segments which were all quite low (Kruskal-Wallis tests; Instruction segments, $p > 0.05$; Go segments, $p < 0,01$; Movement segments, $p < 0.01$; Hold segments, $p < 0.001$). Post-hoc testing showed that in all significant cases (9 cases: 3 CCA coefficients x 3 sets of trajectory segments, Tukey honestly significant difference tests), though the MN:E/O coefficients might not be significantly lower than the corresponding MN/1:2 coefficients and/or significantly higher than the MN/AE coefficients, the MN/AE coefficients were significantly lower than the corresponding MN/1:2 coefficients in all 9 cases. These findings fail to support the hypothesis that during action execution MN and AE neuron trajectory segments would align well, and suggest instead that the patterns of co-modulation among AE neurons during the four different RGM movements did not align with the patterns of co-modulation among MNs.

Did these differences in MN:1/2, MN:E/O, and MN/AE alignment result from consistent differences in their respective patterns of co-modulation, or from of greater trial-by-trial variability in the patterns of co-modulation among MNs during observation than during execution, and still greater variability among AE neurons during execution? The bootstrapping approach we used for CCA (see Methods) enabled us to evaluate the consistency of relationships among trajectory

bioRxiv preprint doi: https://doi.org/10.1101/2023.11.06.565833; this version posted January 5, 2025. The copyright holder for this preprint (which was not certified by peer review) is the author/funder, who has granted bioRxiv a license to display the preprint in perpetuity. It is made available under aCC-BY 4.0 International license.

segments across repeated samplings of trials recorded from the same neuron population in the same session and in the same context (execution or observation). We therefore performed 500 iterations of CCA between two different random samples of MN execution (MN:E/E), MN observation (MN:O/O), or AE execution (AE:E/E) trajectory segments from a given session (2 R, 3 T, 3 F). This within-group alignment of MN execution trajectory segments from the same session (Figure 8D, MN:E/E, gray, Hold: $\overline{CC1} = 0.88$, $\overline{CC2} = 0.74$, $\overline{CC3} = 0.55$) was as strong as between session alignment (Figure 8C, MN/1:2, black). But within-group alignment of MN observation trajectory segments (Figure 8D, MN:O/O, orange, Hold: $\overline{CC1} = 0.65$, $\overline{CC2} = 0.46$, $\overline{CC3} = 0.24$) was lower than that found with MN execution segments (Figure 8C, MN:E/O, red, ($\overline{CC1} = 0.73$, $\overline{CC2} = 0.54$, $\overline{CC3} = 0.39$). Likewise, within-group alignment of AE neuron trajectory segments (Figure 8D, AE:E/E, light blue, Hold: $\overline{CC1} = 0.46$, $\overline{CC2} = 0.25$, $\overline{CC3} = 0.10$) was lower than their alignment with MN execution segments (Figure 8C, MN/AE, blue, Hold: $\overline{CC1} = 0.57$, $\overline{CC2} = 0.35$, $\overline{CC3} = 0.19$). Whereas MN execution trajectories were relatively consistent within sessions, MN observation trajectories and AE execution trajectories were less so.

Statistical comparisons across these three sets of within-group alignments (MN:E/E; MN:O/O; and AE:E/E) showed significant variation in each of the three CCA coefficients for all four trajectory segments (Kruskal-Wallis tests; Instruction segments, $p < 0.05$; Go segments, $p < 0,01$; Movement segments, $p < 0.001$; Hold segments, $p < 0.001$). Post-hoc testing showed that in all significant cases (12 cases: 3 CCA coefficients x 4 sets of trajectory segments, Tukey honestly significant difference tests), though the within-group MN:O/O coefficients might not be significantly lower than the corresponding MN:E/E coefficients and/or significantly higher than the AE:E/E coefficients, the within-group AE:E/E coefficients were significantly lower than the corresponding MN:E/E coefficients in all 12 cases. These findings suggest that the patterns of co-modulation among AE neurons during the four different RGM movements, as well as the patterns of co-modulation among MNs during observation, were more variable from trial to trial than were the patterns of MN co-modulation during execution. This greater trial-to-trial variability in co-modulation of MNs during observation and even greater variability in AE neurons during execution (Figure 8D) likely contributes to the weaker alignment of MN observation segments with MN execution segments and even weaker alignment of AE and MN execution segments (Figure 8C). Whereas the predominant patterns of co-modulation among MNs during the four different RGM movements were relatively consistent, co-modulation among MNs during observation was less consistent, and co-modulation of AE neurons during execution even less so.

bioRxiv preprint doi: https://doi.org/10.1101/2023.11.06.565833; this version posted January 5, 2025. The copyright holder for this preprint (which was not certified by peer review) is the author/funder, who has granted bioRxiv a license to display the preprint in perpetuity. It is made available under aCC-BY 4.0 International license.

DISCUSSION

As neurophysiological studies have advanced from examination of single neurons to neuron populations, analytic approaches have advanced from analyses of single neuron firing rates to analyses of co-modulation patterns among neuron populations. The co-modulation in a neuronal population can be expressed as the trajectory of the simultaneous firing rates of the *N* neurons through their *N*-dimensional state space, and the predominant patterns of co-modulation can be extracted by projecting this high-dimensional trajectory into a low-dimensional subspace that captures a large proportion of the population's firing-rate variance. Previous studies of reaching movements have shown that the low-dimensional population trajectories of PMd and M1 neurons occupy one subspace during a preparatory delay epoch and then transition to a different subspace during the reaching movement per se (Kaufman et al., 2014; Elsayed et al., 2016). Compared to reaching movements, however, the low-dimensional trajectories of neuronal activity controlling hand movements are relatively complex (Rouse and Schieber, 2018; Suresh et al., 2020). To approach this problem, rather than examining neural trajectories in subspaces that capture only a selected epoch of the behavioral task, we identified time series of instantaneous, condition-dependent subspaces covering the entire time course of reach-grasp-manipulate (RGM) behavioral trials that included a preparatory delay epoch.

Using this approach, we found that the instantaneous, condition-dependent subspace of PM MN populations shifts progressively during both execution and observation of RGM trials. The instantaneous subspace of AE neuron populations likewise shifts progressively during action execution. This progressive shifting of the instantaneous subspace resembles that found previously using fractional overlap of condition-dependent variance in M1 neuron populations performing a similar RGM task without a delay epoch (Rouse and Schieber, 2018). Although the progressive shifting described here is a rotation in the mathematical sense, it is not necessarily a smooth rotation in a few dimensions. We therefore have used the word "shift" to contrast with the smooth rotation of neural trajectories in a low-dimensional subspace described in other studies, particularly those using jPCA (Churchland et al., 2012; Russo et al., 2020; Rouse et al., 2022).

Features of the instantaneous subspace

Short bursts of "signal" related discharge are known to occur in a substantial fraction of PMd neurons beginning at latencies of ~60 ms following an instructional stimulus (Weinrich et al., 1984; Cisek and Kalaska, 2004). Here we found that the instantaneous subspace shifted briefly toward the subspace present at the time of instruction onset (I), similarly during execution and observation. This brief trough in principal angle (Figure 4A) and the corresponding peak in classification accuracy (Figure 7A) in part may reflect smoothing of firing rates with a 50 ms Gaussian kernel. We speculate, however, that the early rise of this peak at the time of instruction onset also reflects the anticipatory activity often seen in PMd neurons in expectation of an instruction, which may not be entirely non-specific, but rather may position the neural population to receive one of a limited set of potential instructions (Mauritz and Wise, 1986). We attribute the relatively low amplitude of peak classification accuracy for Instruction trajectory segments to the likely possibility that only the last 40 ms of our 100 ms Instruction segments captured signal related discharge.

bioRxiv preprint doi: https://doi.org/10.1101/2023.11.06.565833; this version posted January 5, 2025. The copyright holder for this preprint (which was not certified by peer review) is the author/funder, who has granted bioRxiv a license to display the preprint in perpetuity. It is made available under aCC-BY 4.0 International license.

The firing rates of MNs in both PMv and PMd have been shown previously to modulate during preparatory delay periods (Cisek and Kalaska, 2004; Maranesi et al., 2014). During execution of a reaching task, condition-dependent subspaces during the preparatory delay are orthogonal to those found during the subsequent movement epochs (Kaufman et al., 2014; Elsayed et al., 2016). Studies that have identified such orthogonal subspaces specifically optimized preparatory and movement subspaces to be orthogonal to one another, however, whereas the present approach did not. Here, we found that during the preparatory delay epoch of the present RGM task, the condition-dependent, instantaneous subspace did not remain orthogonal to that which would be present at movement onset or during the movement epoch. Rather, as the preparatory delay proceeded, the instantaneous subspace shifted concurrently toward both the subspace that would be present at the time of the go cue ending the preparatory delay (G) and that which would be present at movement onset (M). By time G, the instantaneous subspace already had shifted approximately halfway toward the time M subspace. This difference in the orthogonality of preparatory versus movement subspaces may reflect differences in reaching without grasping, which involves coordinated motion in 4 degrees of freedom (DOFs) at the shoulder and elbow, versus the present RGM movements, which involve simultaneous, fluidly coordinated motion in at least 22 DOFs of the shoulder, elbow, wrist, and digits (Rouse and Schieber, 2015). Finally, we note that the progressive shift toward the subspace present at the onset of the final hold (H) did begin only after the delay period had ended (G) and around the time of movement onset (M).

PM MN populations during execution versus observation.

In general, instantaneous execution subspaces were distinct from instantaneous observation subspaces, indicated by the continuously large principal angles between them (Figure 9) and by low classification accuracy when execution trajectories were cross-projected into observation subspaces and vice versa (Figure 10). This was the case not only during corresponding time points in execution and observation trials, but throughout their entire time course. Moreover, in all three monkeys, progressive shifting of the instantaneous, condition-dependent subspace was absent both in the principal angles between execution and observation subspaces and in the decoding of execution trajectory segments cross-projected into observation subspaces (and vice versa). These findings indicate that the predominant modes of co-modulation among PM MNs are largely distinct during execution and observation.

Although mirror neurons originally were thought to provide highly congruent neural representations of action execution and action observation (Gallese et al., 1996; Rizzolatti et al., 1996), the present findings are consistent with recent studies that have emphasized the considerable fraction of neurons with non-congruent activity, as well as differences in neural population activity during action execution versus action observation (Jiang et al., 2020; Pomper et al., 2023). As more situations have been investigated, the number of conditions needed to define a “true” mirror neuron in the strict sense of being entirely congruent has grown, making the duration of such congruence brief and/or its likelihood comparable to chance (Papadourakis and Raos, 2019; Pomper et al., 2023).

We did not attempt to classify neurons in our PM MN populations as strictly congruent, broadly congruent, or non-congruent. Nevertheless, the minimal overlap we found in instantaneous execution and observation subspaces would be consistent with a low degree of congruence in our PM MN populations. Particularly during one session monkey T was an

bioRxiv preprint doi: https://doi.org/10.1101/2023.11.06.565833; this version posted January 5, 2025. The copyright holder for this preprint (which was not certified by peer review) is the author/funder, who has granted bioRxiv a license to display the preprint in perpetuity. It is made available under aCC-BY 4.0 International license.

exception in this regard, showing a considerable degree of overlap between execution and observation subspaces, not unlike the shared subspace found in other studies that identified orthogonal execution and observation subspaces as well (Jiang et al., 2020). Although our microelectrode arrays were placed in similar cortical locations in the three monkeys, by chance monkey T's PM MN population may have included a substantial proportion of congruent neurons.

Alignment of trajectory segments with canonical correlation

Given the complexity of condition-dependent neural trajectories across the entire time course of RGM trials (Figure 3B), rather than attempting to align entire neural trajectories, we applied canonical correlation to trajectory segments clipped for 100 ms following four well-defined behavioral events: Instruction onset, Go cue, Movement onset, and the beginning of the final Hold. In all cases, alignment was poorest for Instruction segments, somewhat higher for Go segments, and strongest for Movement and Hold segments (Figure 8C). This progressive increase in alignment likely reflects a progressive increase in the difference between average neuron firing rates for trials involving different objects (Figure 5) relative to the trial-by-trial variance in firing rate for a given object.

Corresponding neural representations of action execution and observation during task epochs with higher neural firing rates have been described previously in PMd MNs and in PMv MNs using representational similarity analysis RSA (Papadourakis and Raos, 2019). And during force production in eight different directions, neural trajectories of PMd neurons draw similar "clocks" during execution, cooperative execution, and passive observation (Pezzulo et al., 2022). Likewise in the present study, despite execution and observation trajectories progressing through largely distinct subspaces, in all three monkeys execution and observation trajectory segments showed some degree of alignment, particularly the Movement and Hold segments (Figure 8C), indicating similar relationships among the latent dynamic representations of the four RGM movements during execution and observation.

Alignment between trajectory segments of the same PM MN population during execution versus observation in the same session, however, was less than that found between MN execution segments from two different sessions in the same monkey. In part, this may reflect the lower firing rates of PM MNs typically found during observation as compared to execution trials (Ferroni et al., 2021). Alternatively, the lower alignment may reflect more trial-by-trial variability in MN observation segments than in MN execution segments, as indicated by the limited within-group alignment of MN observation trajectory segments (Figure 8D).

Based on the assumption that AE neurons and MNs function as a homogenous neuron population during action execution, we had expected AE and MN execution trajectory segments to align closely. During execution trials, the progression of instantaneous condition-dependent subspaces and of classification accuracy in AE populations was quite similar to that in MN populations. We were surprised to find, therefore, that alignment between execution trajectory segments from AE populations and from the simultaneously recorded MN populations was even lower than alignment between MN execution and observation segments (Figure 8C, blue versus red). Moreover, whereas within-group alignment of MN execution trajectory segments was high, within-group alignment of AE neuron execution trajectory segments was low (Figure 8D, gray versus light blue). These findings indicate that the predominant patterns of co-modulation

bioRxiv preprint doi: https://doi.org/10.1101/2023.11.06.565833; this version posted January 5, 2025. The copyright holder for this preprint (which was not certified by peer review) is the author/funder, who has granted bioRxiv a license to display the preprint in perpetuity. It is made available under aCC-BY 4.0 International license.

among MNs during execution are quite consistent within sessions, but the patterns of co-modulation among AE neurons are considerably more variable. Together with our previous finding that modulation of MNs leads that of non-mirror neurons in time, both at the single neuron level and at the population level (Mazurek and Schieber, 2019), this difference in consistency versus variability leads us to speculate that during action execution, while MNs carry a consistent forward model of the intended movement, AE neurons carry more variable feedback information.

The role of mirror neuron populations

Neither the congruence versus non-congruence of individual MN discharge nor the canonical correlation of population dynamics during execution and observation provide direct causal evidence that MNs mediate understanding of the observed actions of other individuals (Hickok, 2009; Yuste, 2015; Krakauer et al., 2017). Many interpretations of such findings are possible, and testing various hypotheses ultimately may require selective experimental manipulation (e.g. inactivation) of MN activity during observation in ways beyond our current capabilities. Nevertheless, the common finding that large fractions of neurons in both PM and M1 discharge both during execution and during observation makes it unlikely that the discharge of MNs during observation is vestigial, with no meaning for the organism.

Although we did not track extraocular movements, video monitoring demonstrated that our monkeys remained attentive throughout the blocks of observation trials, actively scanning the visual environment. Though perhaps not following the experimenter's movements closely with eye movements, or even with covert visual attention, the present results in and of themselves demonstrate that during observation trials the PM MN population was processing information on the sequential epochs of the behavioral task (Mazurek et al., 2018) as well as the object to which the experimenter's actions were directed on each trial. These findings are consistent with the notion that the PM MN population predictively represents the sequence of behavioral events during observation trials (Kilner et al., 2007; Maranesi et al., 2014; Ferroni et al., 2021). Our finding that within-group alignment of MN observation trajectory segments was lower than that of MN execution segments (Figure 8D), however, indicates more trial-by-trial variability of MN co-modulation during observation than during execution. In addition to any consistent, predictive, forward model of the observed experimenter's expected performance, MNs thus may also receive visual input that incorporates more variable, trial-by-trial deviation from the predicted performance being observed.

One classic interpretation of similar latent dynamics in the PM MN population during execution and observation would be that this similarity provides a means for the brain to recognize similar movements performed by the monkey during execution and by the experimenter during observation. Through some process akin to a communication subspace (Semedo et al., 2019), brain regions beyond PM might recognize the correspondence between the latent dynamics of the executed and observed actions.

Alternatively, given that observation of another individual can be considered a form of social interaction, PM MN population activity during action observation, rather than representing movements made by another individual similar to one's own movements, instead may represent different movements one might execute oneself in response to those made by another individual (Ninomiya et al., 2020; Bonini et al., 2022; Ferrucci et al., 2022; Pomper et al., 2023). This possibility is consistent with the finding that the neural dynamics of PM MN populations are

bioRxiv preprint doi: https://doi.org/10.1101/2023.11.06.565833; this version posted January 5, 2025. The copyright holder for this preprint (which was not certified by peer review) is the author/funder, who has granted bioRxiv a license to display the preprint in perpetuity. It is made available under aCC-BY 4.0 International license.

more similar during observation of biological versus non-biological movements than during execution versus observation (Albertini et al., 2021). Though neurons active only during observation of others (AO units) have been hypothesized to drive observation activity in MNs, the present AO populations were too small to analyze with the approaches we applied here. Nevertheless, the similar relative organization of the execution and observation population activity in PM MNs revealed here by alignment of their latent dynamics through CCA could constitute a correspondence between particular movements that might be made by the subject in response to particular movements made by the other individual, i.e. responsive movements which would not necessarily be motorically similar to the observed movements.

The present analyses as well as others have focused on the condition-dependent variance in MN population activity (Jiang et al., 2020). Other studies that have not separated the condition-dependent versus condition-independent variance in neural activity have described even more similar latent dynamics during execution and observation (Mazurek et al., 2018; Jerjian et al., 2020; Pezzulo et al., 2022). We speculate that condition-dependent activity may represent particular types of movement (e.g. sphere, button, coaxial cylinder, or perpendicular cylinder) in a manner that differs depending on the actor (one's self versus another individual). Concurrently, condition-independent activity may provide a neural representation of a class of action (e.g. RGM movements) independent of the actor.

bioRxiv preprint doi: https://doi.org/10.1101/2023.11.06.565833; this version posted January 5, 2025. The copyright holder for this preprint (which was not certified by peer review) is the author/funder, who has granted bioRxiv a license to display the preprint in perpetuity. It is made available under aCC-BY 4.0 International license.

METHODS

Three Rhesus monkeys, R, T, and F (a 6 kg female, a 10 kg male, and an 11 kg male, *Macaca mulatta*) were used in the present study. All procedures for the care and use of these non-human primates followed the Guide for the Care and Use of Laboratory Animals and were approved by the University Committee on Animal Resources at the University of Rochester, Rochester, New York.

Execution trials

Each monkey was trained to perform a delayed-response Reach-Grasp-Manipulate (RGM) task (Figure 2). Prior to each trial a ring of blue LEDs was illuminated around the pole supporting a center object and a 4 kHz tone began, both signaling the end of an inter-trial interval and the opportunity to begin a new trial. The monkey initiated the following sequence by pulling the center object for an initial hold epoch of randomly varied duration (500-1000 ms). A ring of blue LEDs around the pole supporting one of four peripheral objects then was illuminated instructing the monkey as to the target object for the current trial. After 500 ms these instruction LEDs were extinguished, and the monkey was required to wait for a preparatory delay epoch lasting randomly 500-2000 ms. At the end of this preparatory delay epoch, the blue LEDs for the center object were extinguished and the 4 kHz tone ceased, providing a go cue. The monkey then reached to, grasped, and manipulated the remembered target object: turning a sphere, pushing a button, pulling a coaxial cylinder (coax), or pulling a perpendicular cylinder (perp). The reach, grasp, manipulate sequence was performed as a single, uninterrupted, fluid movement of the entire upper extremity (Rouse and Schieber, 2015, 2016a, b). Once the instructed object had been manipulated, a ring of green LEDs around the object illuminated (indicating successful manipulation of the object) and the ring of blue LEDs for that object also illuminated (indicating correct object). The monkey then was required to hold the instructed object in its manipulated position for a final hold epoch of 1000 ms, after which the blue LEDs were extinguished. (The green LEDs extinguished whenever the monkey released the object.) After a 300 ms delay, the monkey received a liquid reward on each successful trial.

The selection and sequence of target objects in successive trials was controlled by custom software (Unified Task Control System, Gil Rivlis), which also 1) generated behavioral event marker codes (Figure 2B), and 2) arranged trials involving the four different objects in a pseudorandom block design. The behavioral event marker codes indicated the times at which specific behavioral events occurred: Start of trial, Instruction onset, Instruction offset, Go cue (delay epoch ended), Movement onset, Hold began, Hold ended, End of trial. One trial involving each of the four different objects was presented sequentially in a block. Once a block had been completed, the sequence of the four objects was shuffled randomly for the next block. To prevent the monkey from skipping more difficult objects, if the monkey failed to complete a trial successfully the same target was repeated until the monkey succeeded.

Observation trials

In a separate block of trials, the monkey observed an experimenter performing the same delayed-response RGM task. The experimenter occasionally made errors intentionally. The monkey received a reward each time the experimenter performed a successful trial, but not when the experimenter made an error, which kept the monkey attentive to the experimenter's performance. Although extraocular movements were not recorded or controlled, video

bioRxiv preprint doi: https://doi.org/10.1101/2023.11.06.565833; this version posted January 5, 2025. The copyright holder for this preprint (which was not certified by peer review) is the author/funder, who has granted bioRxiv a license to display the preprint in perpetuity. It is made available under aCC-BY 4.0 International license.

798 monitoring verified that the monkey remained alert and attentive throughout blocks of
799 observation trials.

800 **Neuron Recording**

801 The three monkeys each were implanted with Floating Microelectrode Arrays (FMAs,
802 Microprobes for Life Sciences), in the ventral premotor cortex (PMv) and in the dorsal premotor
803 cortex (PMd). In monkeys R and T, 16-channel FMAs were implanted; in monkey F, 32-channel
804 FMAs were used (Figure 2C). Monkeys R and F each had a total of 64 recording electrodes
805 implanted in PMd and 64 in PMv, whereas monkey T had 64 in PMd, but only 48 in PMv.
806 Broadband signals were recorded simultaneously from all 128 electrodes using a Nomad/Trellis
807 data acquisition system (Ripple, Salt Lake City, UT), which also recorded the behavioral event
808 marker codes generated by the behavioral control system. In each recording session, data were
809 collected during similar numbers of successful trials involving each target object during
810 execution and then during observation, as summarized in Table 2. Off-line, spike waveforms
811 were extracted and sorted using custom software (Rouse and Schieber, 2016). Sorted units
812 were classified as definite single units, probably single units, multi-units, or noise based on their
813 signal-to-noise ratio and estimated fraction of false-positive spikes using our previously
814 published criteria. All three types of units were included in the present analyses.

815 **Mirror Neuron Identification**

816 Although many studies have focused on neurons from either PMv or PMd, given that
817 neurons in each area have been shown to be modulated during both reaching and grasping
818 (Stark et al., 2007) and during both execution and observation (Papadourakis and Raos, 2019),
819 we chose to combine units from these two cortical areas for the present analyses. Each unit
820 was tested for task-related modulation. Because a given neuron's firing rates during execution
821 and observation trials almost always differed (Ferroni et al., 2021; Pomper et al., 2023), we
822 tested each unit for modulation using data from these two contexts separately. Spike counts
823 from each successful behavioral trial were extracted during eleven 200 ms periods: i) before
824 instruction onset, ii) after instruction onset, iii) before instruction offset, iv) after instruction offset
825 (delay epoch began), v) before delay ended, vi) after delay ended (reaction epoch began), vii)
826 before movement onset, viii) after movement onset (movement epoch began), ix) before
827 movement ended, x) after movement ended (hold epoch began), xi) before hold ended. We then
828 conducted two-way ANOVA on these spike counts using object and time period as factors. We
829 considered a unit task-related if it showed a significant main effect of either i) object or ii) time
830 period, or a significant iii) interaction effect. Any unit modulated significantly both during
831 execution and during observation was considered to be a mirror neuron (MN). Because each
832 unit thus had six opportunities to show significance, we used a corrected significance criterion of
833 $p<0.0083$ ($<0.05/6$). Any unit modulated during execution but not during observation was
834 considered an action execution (AE) neuron. Any unit modulated during action observation but
835 not during execution was considered an action observation neuron (AO). Units unmodulated
836 during both execution and observation were considered not significantly (NS) related to the task.

837 **Data analysis**

838 Spike times for each neuron were binned (bin width = 1 ms), smoothed with a Gaussian
839 kernel (σ = 50 ms), and square-root transformed to render variance similar from low to high
840 firing rates (Kihlberg et al., 1972; Snedecor and Cochran, 1980). The activity of each neuron
841 was time-aligned to four behavioral events and truncated before and after using the median

bioRxiv preprint doi: https://doi.org/10.1101/2023.11.06.565833; this version posted January 5, 2025. The copyright holder for this preprint (which was not certified by peer review) is the author/funder, who has granted bioRxiv a license to display the preprint in perpetuity. It is made available under aCC-BY 4.0 International license.

delay, reaction, and movement times per object and per session as follows: i) instruction onset (I)—500 ms before to 500 ms after; ii) go cue (G)—median delay duration before to half the median reaction time after; iii) movement onset (M)—half the median reaction time before to 200 ms after; and iv) start of final hold (H)—200 ms before to 200 ms after. These four snippets of neural activity were concatenated for each trial. Neural activity then was stored as a three-dimensional tensor (*N* x *K* x *T*, where *N* is number of neurons, *K* the number of trials, and *T* the number of time points) for each of the four target objects.

Instantaneous subspace identification

Instantaneous neural subspaces were identified at 1 ms intervals. At each 1 ms time step, the *N*-dimensional neural firing rates from trials involving the four different objects—sphere, button, coaxial cylinder, and perpendicular cylinder—were averaged separately, providing four points in the *N*-dimensional space representing the average neural activity for trials involving the different objects at that time step. PCA then was performed on these four points. Because three dimensions capture all the variance of four points, three principal component dimensions fully defined each instantaneous subspace. Each instantaneous 3D subspace can be considered a filter described by a matrix, W, that can project high-dimensional neural activity into a low-dimensional subspace, with the time series of instantaneous subspaces, W_i, forming a time series of filters (Figure 1B).

Trajectory visualization and separation

We projected 100 ms segments of neural activity into each instantaneous subspace by multiplying the neural activity, $X(t)$, by the transforming matrix for the i^{th} subspace, W_i ,which yielded low dimensional trajectories, $L(t) = X(t)W_i \ (t \in T)$. This process was repeated for each instantaneous subspace in the time domain of interest. To quantify the separation between the four trial-averaged trajectory segments involving the different objects in a given instantaneous subspace, we then calculated their cumulative separation (CS) as:

$$CS = \frac{1}{T}\sum_{t\in T} D(t) = \frac{1}{T}\sum_{t\in T}\sum_{i\neq j} d_{ij}(t)$$

where $d_{ij}(t)$ is the 3-dimensional Euclidean distance between the i^{th} and j^{th} trajectories at time point t. We summed the 6 pairwise distances between the 4 trajectory segments across time points and normalized by the number of time points, $T = 100$. The larger the CS, the greater the separation of the trajectory segments.

Subspace Comparisons—Principal Angles

To assess the progressive shift of instantaneous subspaces, we computed the principal angles (Bjorck and Golub, 1973; Gallego et al., 2018) between the instantaneous subspace at each of four selected time points—onset of the instruction (I), go cue (G), onset of movement (M), and beginning of the final hold (H)—and each of the other instantaneous subspaces in a time series. For example, given the 3-dimensional instantaneous subspace at the time of movement onset, W_M, and at any other time, W_i, we calculated their 3x3 inner product matrix and performed singular value decomposition to obtain:

$$W_M^T W_i = P_M C P_i^T$$

bioRxiv preprint doi: https://doi.org/10.1101/2023.11.06.565833; this version posted January 5, 2025. The copyright holder for this preprint (which was not certified by peer review) is the author/funder, who has granted bioRxiv a license to display the preprint in perpetuity. It is made available under aCC-BY 4.0 International license.

where 3x3 matrices P_M and P_i define new manifold directions which successively minimize the 3 principal angles specific to the two subspaces being compared. The elements of diagonal matrix C then are the ranked cosines of the principal angles, θ_i , ordered from smallest to largest:

$$C = diag(\cos(\theta_1), \cos(\theta_2), \cos(\theta_3)) .$$

In Figure 4 – figure supplement 1, using all trials from monkey R, session 1, we have plotted the three principal angles as a function of time. Note that at time when $W_i = W_M$, all three principal angles are zero by definition, and the sharp decline before time M and the sharp rise afterward reflect the Gaussian kernel (σ = 50 ms) used to smooth unit firing rates. These sharp troughs thus are trivial, but both the gradual decline before and the gradual rise following the sharp troughs are not. Given that the set of three principal angles typically followed similar time courses, in the Results we illustrate only the first principal angle, θ_1 .

Furthermore, to provide some indication of the degree of variability in the first principal angle, we randomly selected 20 trials involving each target object (totaling 80 trials) with replacement and calculated the first principal angle as a function of time, repeating this process 10 times. The results, shown in Figures 4, 7, Figure 4 – figure supplement 3, and Figure 7 – figures supplement 2 are presented as the mean ±1 standard deviation across these 10-fold cross-validations. Note that this mean never reaches zero because the instantaneous subspaces at times I, G, M, and H were computed using all the available trials.

In the example of Figure 4 – figure supplement 1, the first principal angle never reached 90° either. To determine whether this reflected a lack of orthogonality or a limitation of population size, we computed the first principal angle between a fixed 3-dimensional subspace, and 5000 3-dimensional subspaces randomly chosen from *N*-dimensional spaces, for *N* varying from 5 to 500. Figure 4 – figure supplement 2 shows that for large *N*, principal angles between a fixed subspace and other randomly chosen subspaces are likely to be close to 90°. But as *N* decreases, these random principal angles are less likely to approach 90°, without necessarily indicating non-random overlap of the subspaces. In Figures 4, 7, Figure 4 – figure supplement 3, and Figure 7 – figures supplement 2, we therefore indicate levels of principal angles that might arise by chance alone using the smallest *N* from any of the 3 sessions for a given monkey (see Table 2).

Decodable information—LSTM

As illustrated schematically in Figure 1B, the same segment of high-dimensional neural activity projected into different instantaneous subspaces can generate low-dimensional trajectories of varying separation. The degree of separation among the projected trajectory segments will depend, not only on their separation at the time when the segments were clipped, but also on the similarity of the subspaces into which the trajectory segments are projected. To quantify the combined effects of trajectory separation and projection into different subspaces, we projected high-dimensional neural trajectory segments (each including 100 points at 1 ms intervals) from successful trials involving each of the four different target objects into time series of 3-dimensional instantaneous subspaces at 50 ms intervals. In each of these instantaneous subspaces, the neural trajectory segment from each trial thus became a 100 point x 3 dimensional matrix. For each instantaneous subspace in the time series, we then trained a separate long short-term memory (LSTM, (Hochreiter and Schmidhuber, 1997)) classifier to attribute each of the neural trajectories from individual trials to one of the four target object labels: sphere, button, coaxial cylinder, or perpendicular cylinder. Using MATLAB's Deep

bioRxiv preprint doi: https://doi.org/10.1101/2023.11.06.565833; this version posted January 5, 2025. The copyright holder for this preprint (which was not certified by peer review) is the author/funder, who has granted bioRxiv a license to display the preprint in perpetuity. It is made available under aCC-BY 4.0 International license.

Learning Toolbox, each LSTM classifier had 3 inputs (instantaneous subspace dimensions), 20 hidden units in the bidirectional LSTM layer, and a softmax layer preceding the classification layer which had 4 output classes (target objects). The total number of successful trials available in each session for each object is given in Table 1. To avoid bias based on the total number of successful trials, we used the minimum number of successful trials across the four objects in each session, selecting that number from the total available randomly with replacement. Each LSTM classifier was trained with MATLAB's adaptive moment estimation (Adam) optimizer on 40% of the selected trials, and the remaining 60% were decoded by the trained classifier. The success of this decoding was used as an estimate of classification accuracy from 0 (no correct classifications) to 1 (100% correct classifications). This process was repeated 10 times and the mean ± standard deviation across the 10 folds was reported as the classification accuracy at that time. Classification accuracy of trials projected into each instantaneous subspace at 50 ms intervals was plotted as a function of trial time.

Similarity of aligned latent dynamics

We used Canonical Correlation Alignment (CCA) to compare the similarity of latent dynamics in different subspaces (Gallego et al., 2020). In brief, given latent dynamics (trajectory segments) in two original subspaces, L_A and L_B, CCA finds a linear transformation of each original subspace such that, when projected into a common subspace, the aligned latent dynamics, $\tilde{L}_A$ and $\tilde{L}_B$, are maximumly correlated in each dimension of the common subspace. Larger canonical correlation coefficients (CCs) indicate a higher degree of alignment.

CCA was performed as follows: The original latent dynamics, L_A and L_B, first were transformed and decomposed as $L_A^T = Q_A R_A$ and $L_B^T = Q_B R_B$. The first *m = 3* column vectors of each Q_i provide an orthonormal basis for the column vectors of L_i^T (where $i = A, B$). Singular value decomposition on the inner product matrix of Q_A and Q_B then gives $Q_A^T Q_B = USV^T$, and new manifold directions that maximize pairwise correlations are provided by $M_A = R_A^{-1}U$ and $M_B = R_B^{-1}V$. We then projected the original latent dynamics into the new, common subspace: $\tilde{L}_A^T = L_A^T M_A$; $\tilde{L}_B^T = L_B^T M_B$. Pairwise correlation coefficients between the aligned latent dynamics sorted from largest to smallest then are given by the elements of the diagonal matrix $S = \tilde{L}_A \tilde{L}_B^T$.

To provide an estimate of variability, we used a bootstrapping approach to CCA. From each of two data sets we randomly selected 20 trials involving each target object (totaling 80 trials) with replacement, clipped trajectory segments from each of those trials for 100 ms (100 points at 1 ms intervals) after the instruction onset, go cue, movement onset, or beginning of the final hold, and performed CCA as described above. (Note that because session 1 from monkey R included only 8 button trials (Table 1), we excluded this session from CCA analyses.) With 500 iterations, we obtained a distribution of the correlation coefficients (CCs) between the two data sets in each of the three dimensions of the aligned subspace, which permitted statistical comparisons. We then used this approach to evaluate alignment of latent dynamics between different sessions (e.g. execution trials on two different days), between different contexts (e.g. execution and observation), and between different neural populations (e.g. MNs and AE neurons).This bootstrapping approach further enabled us to assess the consistency of relationships among neural trajectories within a given group—i.e. the same neural population during the same context (execution or observation) in the same session—by drawing two separate random samples of 80 trials from the same population, context, and session (Figure 8D), which would not have been possible had we concatenated trajectory segments from all trials in the session (Gallego et al., 2020; Safaie et al., 2023).

bioRxiv preprint doi: https://doi.org/10.1101/2023.11.06.565833; this version posted January 5, 2025. The copyright holder for this preprint (which was not certified by peer review) is the author/funder, who has granted bioRxiv a license to display the preprint in perpetuity. It is made available under aCC-BY 4.0 International license.

Code Availability

Code packages for all analyses performed in this work are available at: https://github.com/ShiftingSubspace/shiftsubs .

bioRxiv preprint doi: https://doi.org/10.1101/2023.11.06.565833; this version posted January 5, 2025. The copyright holder for this preprint (which was not certified by peer review) is the author/funder, who has granted bioRxiv a license to display the preprint in perpetuity. It is made available under aCC-BY 4.0 International license.

973 **REFERNCES**

974

975 Albertini D, Lanzilotto M, Maranesi M, Bonini L (2021) Largely shared neural codes for biological
976 and nonbiological observed movements but not for executed actions in monkey
977 premotor areas. J Neurophysiol 126:906-912.
978 Ames KC, Ryu SI, Shenoy KV (2014) Neural dynamics of reaching following incorrect or absent
979 motor preparation. Neuron 81:438-451.
980 Bjorck A, Golub GH (1973) Numerical Methods for Computing Angles between Linear
981 Subspaces. Math Comput 27:579-594.
982 Bonini L, Rotunno C, Arcuri E, Gallese V (2022) Mirror neurons 30 years later: implications and
983 applications. Trends Cogn Sci 26:767-781.
984 Churchland MM, Cunningham JP, Kaufman MT, Foster JD, Nuyujukian P, Ryu SI, Shenoy KV
985 (2012) Neural population dynamics during reaching. Nature 487:51-56.
986 Cisek P, Kalaska JF (2004) Neural correlates of mental rehearsal in dorsal premotor cortex.
987 Nature 431:993-996.
988 Cunningham JP, Yu BM (2014) Dimensionality reduction for large-scale neural recordings. Nat
989 Neurosci 17:1500-1509.
990 Dekleva BM, Chowdhury RH, Batista AP, Chase SM, Yu BM, Boninger ML, Collinger JL (2024)
991 Motor cortex retains and reorients neural dynamics during motor imagery. Nat Hum
992 Behav.
993 di Pellegrino G, Fadiga L, Fogassi L, Gallese V, Rizzolatti G (1992) Understanding motor
994 events: a neurophysiological study. Experimental Brain Research 91:176-180.
995 Dushanova J, Donoghue J (2010) Neurons in primary motor cortex engaged during action
996 observation. Eur J Neurosci 31:386-398.
997 Elsayed GF, Lara AH, Kaufman MT, Churchland MM, Cunningham JP (2016) Reorganization
998 between preparatory and movement population responses in motor cortex. Nat Commun
999 7:13239.
1000 Ferroni CG, Albertini D, Lanzilotto M, Livi A, Maranesi M, Bonini L (2021) Local and system
1001 mechanisms for action execution and observation in parietal and premotor cortices. Curr
1002 Biol 31:2819-2830 e2814.
1003 Ferrucci L, Nougaret S, Falcone R, Cirillo R, Ceccarelli F, Genovesio A (2022) Dedicated
1004 Representation of Others in the Macaque Frontal Cortex: From Action Monitoring and
1005 Prediction to Outcome Evaluation. Cereb Cortex 32:891-907.
1006 Gallego JA, Perich MG, Miller LE, Solla SA (2017) Neural Manifolds for the Control of
1007 Movement. Neuron 94:978-984.
1008 Gallego JA, Perich MG, Chowdhury RH, Solla SA, Miller LE (2020) Long-term stability of cortical
1009 population dynamics underlying consistent behavior. Nat Neurosci 23:260-270.
1010 Gallego JA, Perich MG, Naufel SN, Ethier C, Solla SA, Miller LE (2018) Cortical population
1011 activity within a preserved neural manifold underlies multiple motor behaviors. Nature
1012 Communications In Press:1-13.
1013 Gallese V, Fadiga L, Fogassi L, Rizzolatti G (1996) Action recognition in the premotor cortex.
1014 Brain 119:593-609.
1015 Hickok G (2009) Eight problems for the mirror neuron theory of action understanding in
1016 monkeys and humans. J Cogn Neurosci 21:1229-1243.
1017 Hochreiter S, Schmidhuber J (1997) Long short-term memory. Neural Comput 9:1735-1780.
1018 Jerjian SJ, Sahani M, Kraskov A (2020) Movement initiation and grasp representation in
1019 premotor and primary motor cortex mirror neurons. Elife 9.

bioRxiv preprint doi: https://doi.org/10.1101/2023.11.06.565833; this version posted January 5, 2025. The copyright holder for this preprint (which was not certified by peer review) is the author/funder, who has granted bioRxiv a license to display the preprint in perpetuity. It is made available under aCC-BY 4.0 International license.

Jiang X, Saggar H, Ryu SI, Shenoy KV, Kao JC (2020) Structure in Neural Activity during Observed and Executed Movements Is Shared at the Neural Population Level, Not in Single Neurons. Cell Rep 32:108006.

Kaufman MT, Churchland MM, Ryu SI, Shenoy KV (2014) Cortical activity in the null space: permitting preparation without movement. Nat Neurosci 17:440-448.

Kaufman MT, Seely JS, Sussillo D, Ryu SI, Shenoy KV, Churchland MM (2016) The Largest Response Component in the Motor Cortex Reflects Movement Timing but Not Movement Type. eNeuro 3.

Kihlberg JK, Herson JH, Schotz WE (1972) Square Root Transformation Revisited. J Roy Stat Soc C-App 21:76-&.

Kilner JM, Friston KJ, Frith CD (2007) Predictive coding: an account of the mirror neuron system. Cogn Process 8:159-166.

Kobak D, Brendel W, Constantinidis C, Feierstein CE, Kepecs A, Mainen ZF, Qi XL, Romo R, Uchida N, Machens CK (2016) Demixed principal component analysis of neural population data. Elife 5.

Krakauer JW, Ghazanfar AA, Gomez-Marin A, MacIver MA, Poeppel D (2017) Neuroscience Needs Behavior: Correcting a Reductionist Bias. Neuron 93:480-490.

Kraskov A, Dancause N, Quallo MM, Shepherd S, Lemon RN (2009) Corticospinal neurons in macaque ventral premotor cortex with mirror properties: a potential mechanism for action suppression? Neuron 64:922-930.

Kraskov A, Philipp R, Waldert S, Vigneswaran G, Quallo MM, Lemon RN (2014) Corticospinal mirror neurons. Philos Trans R Soc Lond B Biol Sci 369:20130174.

Maranesi M, Livi A, Fogassi L, Rizzolatti G, Bonini L (2014) Mirror neuron activation prior to action observation in a predictable context. J Neurosci 34:14827-14832.

Mauritz KH, Wise SP (1986) Premotor cortex of the rhesus monkey: neuronal activity in anticipation of predictable environmental events. Experimental Brain Research 61:229-244.

Mazurek KA, Schieber MH (2019) Mirror neurons precede non-mirror neurons during action execution. J Neurophysiol 122:2630-2635.

Mazurek KA, Rouse AG, Schieber MH (2018) Mirror Neuron Populations Represent Sequences of Behavioral Epochs During Both Execution and Observation. J Neurosci 38:4441-4455.

Natraj N, Silversmith DB, Chang EF, Ganguly K (2022) Compartmentalized dynamics within a common multi-area mesoscale manifold represent a repertoire of human hand movements. Neuron 110:154-+.

Ninomiya T, Noritake A, Kobayashi K, Isoda M (2020) A causal role for frontal cortico-cortical coordination in social action monitoring. Nat Commun 11:5233.

Papadourakis V, Raos V (2019) Neurons in the Macaque Dorsal Premotor Cortex Respond to Execution and Observation of Actions. Cereb Cortex 29:4223-4237.

Pezzulo G, Donnarumma F, Ferrari-Toniolo S, Cisek P, Battaglia-Mayer A (2022) Shared population-level dynamics in monkey premotor cortex during solo action, joint action and action observation. Prog Neurobiol 210:102214.

Pomper JK, Shams M, Wen S, Bunjes F, Thier P (2023) Non-shared coding of observed and executed actions prevails in macaque ventral premotor mirror neurons. Elife 12.

Rizzolatti G, Craighero L (2004) The mirror-neuron system. Annual Review of Neuroscience 27:169-192.

Rizzolatti G, Fadiga L, Gallese V, Fogassi L (1996) Premotor cortex and the recognition of motor actions. Brain Research Cognitive Brain Rese:131-141.

Rouse AG, Schieber MH (2015) Spatiotemporal distribution of location and object effects in reach-to-grasp kinematics. J Neurophysiol 114:3268-3282.

bioRxiv preprint doi: https://doi.org/10.1101/2023.11.06.565833; this version posted January 5, 2025. The copyright holder for this preprint (which was not certified by peer review) is the author/funder, who has granted bioRxiv a license to display the preprint in perpetuity. It is made available under aCC-BY 4.0 International license.

Rouse AG, Schieber MH (2016a) Spatiotemporal distribution of location and object effects in the electromyographic activity of upper extremity muscles during reach-to-grasp. J Neurophysiol 115:3238-3248.

Rouse AG, Schieber MH (2016b) Spatiotemporal Distribution of Location and Object Effects in Primary Motor Cortex Neurons during Reach-to-Grasp. J Neurosci 36:10640-10653.

Rouse AG, Schieber MH (2018) Condition-Dependent Neural Dimensions Progressively Shift during Reach to Grasp. Cell Rep 25:3158-3168 e3153.

Rouse AG, Schieber MH, Sarma SV (2022) Cyclic, Condition-Independent Activity in Primary Motor Cortex Predicts Corrective Movement Behavior. eNeuro 9.

Russo AA, Khajeh R, Bittner SR, Perkins SM, Cunningham JP, Abbott LF, Churchland MM (2020) Neural Trajectories in the Supplementary Motor Area and Motor Cortex Exhibit Distinct Geometries, Compatible with Different Classes of Computation. Neuron 107:745-758 e746.

Safaie M, Chang JC, Park J, Miller LE, Dudman JT, Perich MG, Gallego JA (2023) Preserved neural dynamics across animals performing similar behaviour. Nature 623:765-771.

Semedo JD, Zandvakili A, Machens CK, Yu BM, Kohn A (2019) Cortical Areas Interact through a Communication Subspace. Neuron 102:249-259 e244.

Shenoy KV, Sahani M, Churchland MM (2013) Cortical control of arm movements: a dynamical systems perspective. Annu Rev Neurosci 36:337-359.

Snedecor GW, Cochran WG (1980) Statistical Methods, 7 Edition. Ames: Iowa State University Press.

Sobinov AR, Bensmaia SJ (2021) The neural mechanisms of manual dexterity. Nat Rev Neurosci 22:741-757.

Stark E, Asher I, Abeles M (2007) Encoding of reach and grasp by single neurons in premotor cortex is independent of recording site. J Neurophysiol 97:3351-3364.

Suresh AK, Goodman JM, Okorokova EV, Kaufman M, Hatsopoulos NG, Bensmaia SJ (2020) Neural population dynamics in motor cortex are different for reach and grasp. Elife 9.

Vigneswaran G, Philipp R, Lemon RN, Kraskov A (2013) M1 corticospinal mirror neurons and their role in movement suppression during action observation. Curr Biol 23:236-243.

Vyas S, Golub MD, Sussillo D, Shenoy KV (2020) Computation Through Neural Population Dynamics. Annual Review of Neuroscience, Vol 43 43:249-275.

Weinrich M, Wise SP, Mauritz KH (1984) A neurophysiological study of the premotor cortex in the rhesus monkey. Brain 107:385-414.

Yuste R (2015) From the neuron doctrine to neural networks. Nat Rev Neurosci 16:487-497.

bioRxiv preprint doi: https://doi.org/10.1101/2023.11.06.565833; this version posted January 5, 2025. The copyright holder for this preprint (which was not certified by peer review) is the author/funder, who has granted bioRxiv a license to display the preprint in perpetuity. It is made available under aCC-BY 4.0 International license.

Figure Supplements

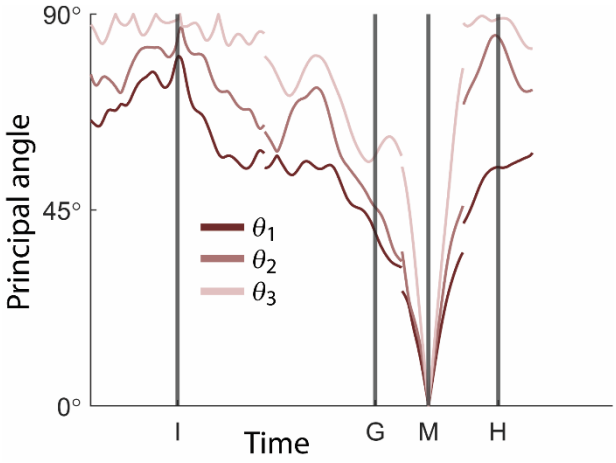

Figure 4 – figure supplement 1. First, second, and third principal angles as a function of time. An example in which the three principal angles, $\theta_1, \theta_2, \theta_3$, between the instantaneous subspace at time M (movement onset) and the entire time series of instantaneous subspaces have been plotted as a function of time for PM MNs. (Data from monkey R, session 1.) Note that all three principal angles go to 0°at time M when the current instantaneous subspace is, by definition, the subspace at time M.

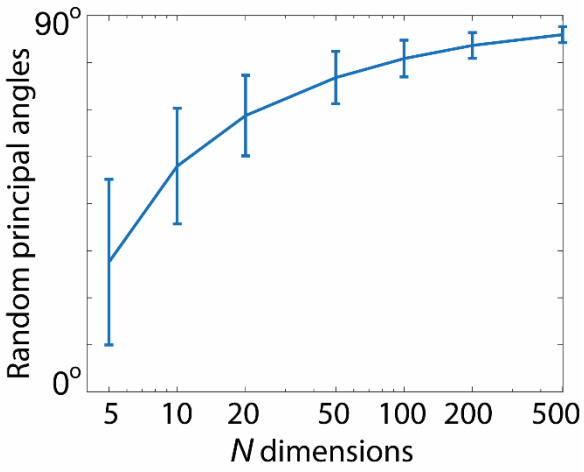

Figure 4 – figure supplement 2. First principal angles between a fixed 3D subspace and 5000 other 3D subspaces randomly chosen from spaces of dimensionality, *N*, varying from 5 to 500. Error bars indicate ± 1 standard deviation from the mean. Note that as the dimensionality of the parent space decreases, the random principal angle also decreases.

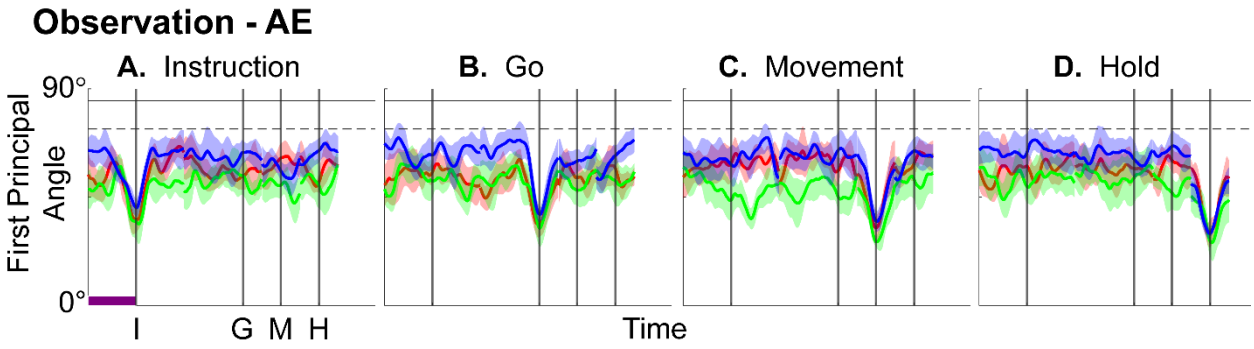

Figure 4 – figure supplement 3. Time course of the first principal angle of instantaneous subspaces for AE neurons during observation trials. As would be expected given that AE neurons were not modulated significantly during observation trials, in the observation context AE populations had no gradual changes in principal angle, showing only relatively sharp troughs dipping toward 0° at each of the four selected times when the current instantaneous subspace, by definition, approached that at times I, G, M, or H. Formatting is the same as in Figure 4.

bioRxiv preprint doi: https://doi.org/10.1101/2023.11.06.565833; this version posted January 5, 2025. The copyright holder for this preprint (which was not certified by peer review) is the author/funder, who has granted bioRxiv a license to display the preprint in perpetuity. It is made available under aCC-BY 4.0 International license.

1109

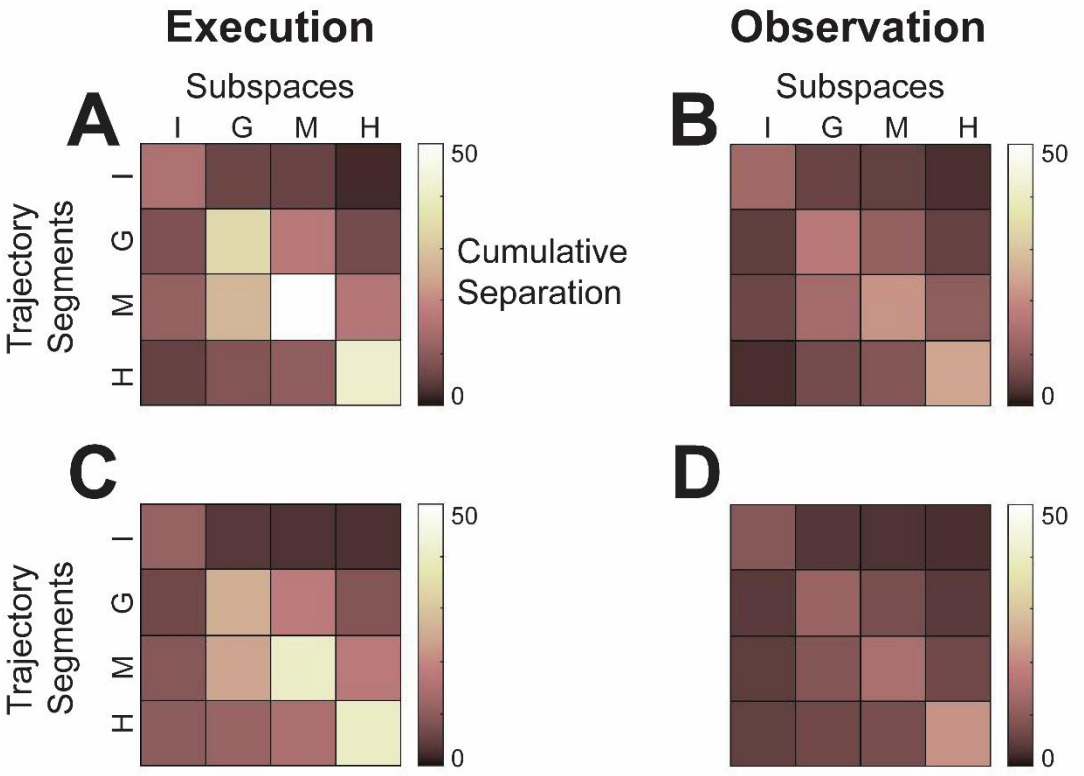

Figure 5 – figure supplement 1. Cumulative separation. To summarize the changes in trajectory separation illustrated in Figure 5, we calculated the 3-dimensional cumulative separation (*CS*, the summed pointwise Euclidean distance between all pairwise combinations of the four object-specific trajectory segments, see Methods) for each set of four segments projected into each of the four instantaneous subspaces at times I, G, M, or H. *CS* values, which we use only to characterize the phenomenon of trajectory separation, are illustrated for execution from the example session of Figure 5 as a color matrix in **A**, and for observation in **B**. For both execution and observation, the highest *CS* values lie on the main diagonal, increasing in temporal order from Instruction to Go to Movement to Hold, with the exception that for execution, *CS* for Hold was less than for Movement. **C** and **D** show *CS* matrices averaged across all three sessions from all three monkeys for execution and observation, respectively, demonstrating that the features seen in the example session of Figure 5 were relatively consistent across sessions. Across all nine sessions two-way ANOVA showed significant main effects on *CS* values of both segment and subspace as well as a significant interaction effect during both execution and observation ($p < 0.05$). In both of these contexts, as the instantaneous subspace of the PM MN population shifted progressively over the time course of RGM trials, the separation of condition-dependent neural trajectories also increased.

1110

bioRxiv preprint doi: https://doi.org/10.1101/2023.11.06.565833; this version posted January 5, 2025. The copyright holder for this preprint (which was not certified by peer review) is the author/funder, who has granted bioRxiv a license to display the preprint in perpetuity. It is made available under aCC-BY 4.0 International license.

1111

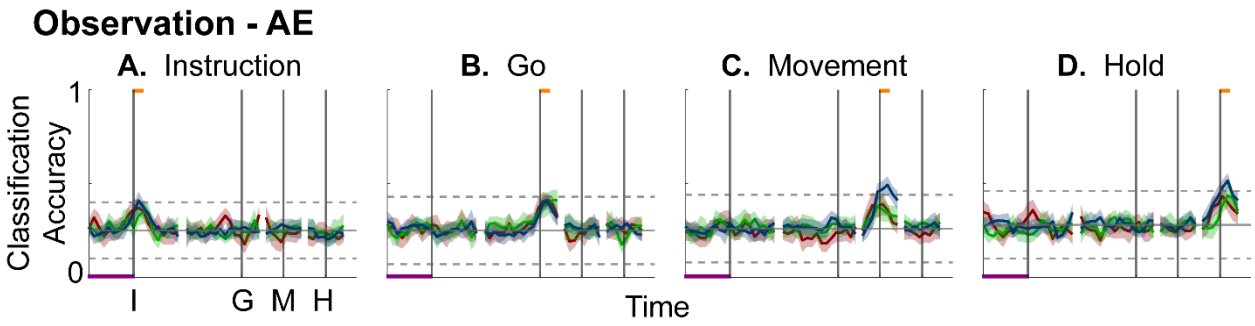

Figure 6 – figure supplement 1. Decodable information as a function of time in PM AE neuron populations. Formatting is the same as in Figure 6. As might have been expected, AE populations showed little if any decodable information during observation.

1112

bioRxiv preprint doi: https://doi.org/10.1101/2023.11.06.565833; this version posted January 5, 2025. The copyright holder for this preprint (which was not certified by peer review) is the author/funder, who has granted bioRxiv a license to display the preprint in perpetuity. It is made available under aCC-BY 4.0 International license.

1113

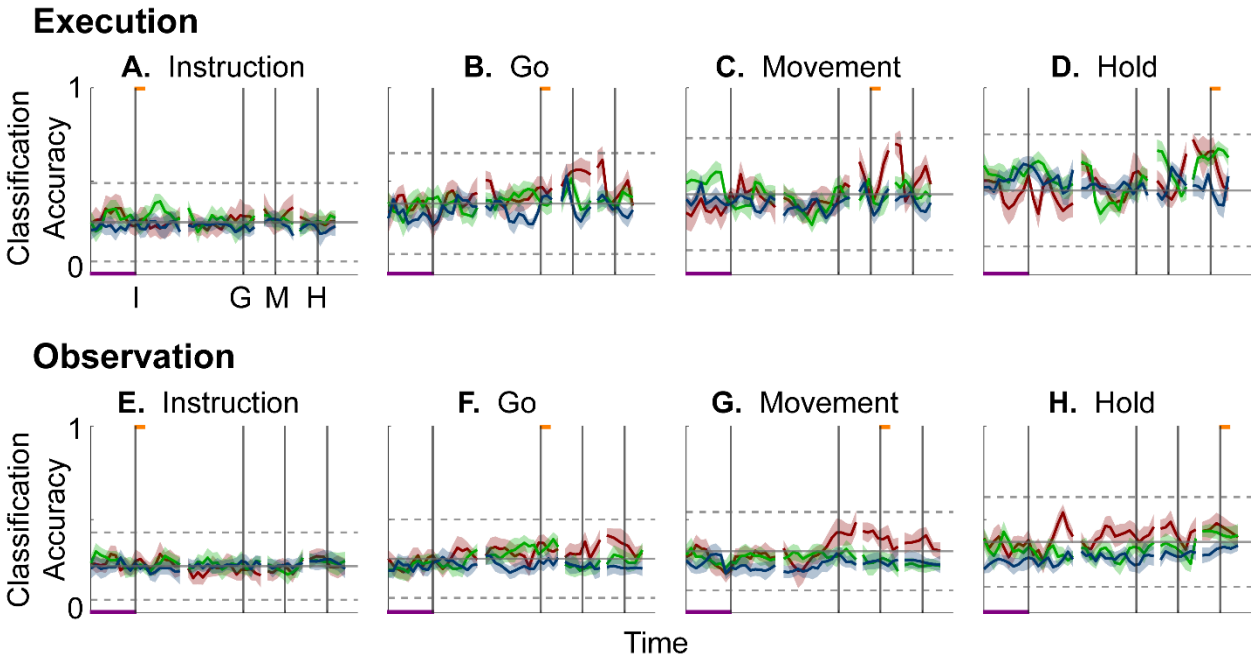

Figure 7 – figure supplement 1. Classification accuracy of trajectory segments cross-projected between instantaneous execution and observation subspaces of PM MNs as a function of time. On top, Instruction, Go, Movement, and Hold *execution trajectory segments* (**A, B, C, D,** respectively) from individual trials have projected into the time series of *instantaneous observation subspaces* and classified with a separate LSTM decoder at each time point; below, Instruction, Go, Movement, and Hold *observation trajectory segments* (**E, F, G, H,** respectively) have been projected into the time series of *instantaneous execution subspaces* and classified. Neither of these cross-projections showed gradual progression to peaks of classification accuracy. Nor did the classification accuracy in either cross-projection exceed that expected from chance alone (horizontal dashed lines). These results confirm that little if any overlap between instantaneous, condition-dependent execution and observation subspaces was present in monkey R. Findings were similar in monkey F. Formatting is the same as in Figure 6.

1114

bioRxiv preprint doi: https://doi.org/10.1101/2023.11.06.565833; this version posted January 5, 2025. The copyright holder for this preprint (which was not certified by peer review) is the author/funder, who has granted bioRxiv a license to display the preprint in perpetuity. It is made available under aCC-BY 4.0 International license.

1115

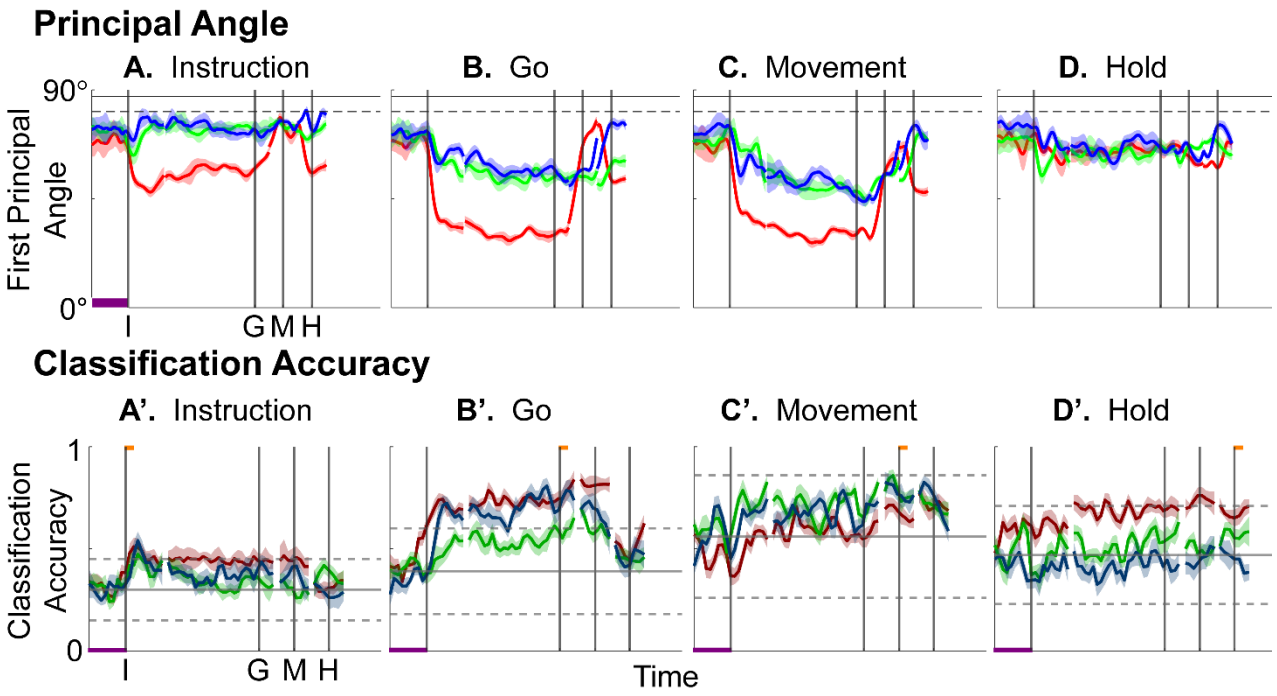

Figure 7 – figure supplement 2. Partial overlap of execution and observation subspaces in monkey T. **A-D**. The first principal angles between the instantaneous *execution* subspace at times I, G, or M (though not H) and the time series of instantaneous *observation* subspaces showed an abrupt drop beginning at the time of instruction onset (I) and continuing until the time of movement onset (M). This drop, which reflects partial overlap of the execution and observation subspaces, was marked during session 1 (red), but less so during sessions 2 and 3 (green and blue, respectively). **A'-D'**. Likewise, Instruction, Go, or Movement, *execution trajectory segments* projected into the time series of *instantaneous observation subspaces* showed a rise in decodable information, also indicative of some degree of overlap, beginning at the time of instruction onset (I). **A-D** are formatted as Figure 4; **A'-D'** as in Figure 6. Overlap like that seen here in monkey T was not found in monkeys R or F.

1116